# Online adaptive equivalent consumption minimization strategy for fuel cell hybrid electric vehicle considering power sources degradation

Huan Li, Alexandre Ravey, Abdoul Diaye, Abdesslem Djerdir

# Online adaptive equivalent consumption minimization strategy for fuel cell hybrid electric vehicle considering power sources degradation

Huan Li[a,b,*], Alexandre Ravey[a,b], Abdoul N'Diaye[a,b], Abdesslem Djerdir[a,b]

[a] *FEMTO-ST, CNRS, Univ. Bourgogne Franche-Comte, UTBM*
[b] *FCLAB, CNRS, Univ. Bourgogne Franche-Comte*

**Abstract**

The aim of this paper is to present an on-line adaptive equivalent consumption minimum strategy (AECMS) for fuel cell hybrid electric vehicle powered by fuel cell, battery and supercapacitor. In order to design the AECMS, an equivalent consumption minimum strategy (ECMS) without considering power sources degradation is firstly designed to decrease hydrogen consumption and degradation of power sources, which chooses fuel cell as the main power source to supply steady power, battery as the main energy storage source to buffer energy demand by vehicle and supercapacitor as the peak power supplier. A testbench is built to validate the developed ECMS. By contrastive experimental tests on ECMS, Rule Based Control Strategy (RBCS) and a Hybrid ECMS Operating mode control Strategy (HEOS) through the built test bench, hydrogen consumption of ECMS decreases 2.16% and 1.47% respectively and it also has the smoothest fuel cell current. Along with the degradation of fuel cell and battery, the charge sustenance objective of battery cannot be reached. Therefore, AECMS is finally designed to adjust equivalent factors and fuel cell dynamic current change rate along with the state of health (SOH) of fuel cell and battery, to make sure the charge sustenance of battery and prolong the lifetime of fuel cell. The method that on-line estimates their SOHs and the effects of their

*Corresponding author
*Email address:* huan.li@utbm.fr (Huan Li)

degradation on ECMS are also analyzed.

*Keywords:* Fuel cell hybrid electric vehicles (FCHEVs), Adaptive equivalent consumption minimum strategy (AECMS), Degradation of power sources, Experimental validation, Online estimation of SOH

---

**Nomenclature**

| | |
|---|---|
| $F$ | Faraday constant |
| $I_{FC}$ | Fuel cell current |
| $m_{BA}$ | Battery equivalent hydrogen consumption |
| $m_{FC}$ | Fuel cell hydrogen consumption |
| $m_{SC}$ | Supercapacitor equivalent hydrogen consumption |
| $N_{cell}$ | The cell number of fuel cell stack |
| $P_{BA}$ | Battery output power |
| $P_{FC}$ | Fuel cell power |
| $P_{SC}$ | Supercapacitor output power |
| $R$ | Ideal gas constant |
| $SOH_{BA}$ | Battery SOH |
| $SOH_{FC}$ | Fuel cell SOH |
| $T$ | The temperature of fuel cell |
| $V_{FC}$ | Fuel cell voltage |

## 1. Introduction

Global warming, air pollution and exhaustion of fossil fuel are gradually attracting people's concern on environmental problems and energy crisis. Fuel cell hybrid electric vehicle (FCHEV) chooses fuel cell and energy storage sources (ESSs) as the power sources, takes hydrogen energy as the fuel and has no air pollutants, which make it a good candidate to solve these problems [1]. Compared to other kinds of fuel cell, proton exchange membrane fuel cell (PEMFC) has many advantages such as high power density, high efficiency and lower operating temperature, which makes it suitable for vehicle application [2]. Fast dynamic power requirement on fuel cell increases its degradation and leads to its fast failure, therefore ESSs are needed to hold the high frequency parts of power to let PEMFC supply steady power. Lithium-ion battery on account of its high energy density can be used as the main energy storage source of FCHEV. Supercapacitor has high power density, which is the great choice of peaking power device. Therefore, Lithium-ion battery and supercapacitor are chosen as the hybrid storage system for the FCHEV in this paper.

An energy management strategy (EMS) is needed to split the power demand among different power sources based on their special characteristics. EMSs can be classified as rule based control strategy (RBCS) and optimization based control strategy [3]. RBCS, including deterministic rule based strategy (DRBS), frequency based strategy and fuzzy rule based strategy (FRBS), depends on a set of rules to determine the control actions at each sample time [4, 5]. Thermostat control strategy [6], load following strategy [7], PID control approach [8], operating mode control [9, 10], stiffness coefficient mode [11] and state machine strategy [12] all belong to DRBS and have ever been used as the EMS of FCHEV. DRBS relies on deterministic rules to control the split of power requirement among different power sources, which are designed according to the designer's experience. FRBS is similar to DRBS. But its rules are in form of "if -then" and its states are described by different membership functions [13, 14]. Frequency based strategy is designed based upon different dynamic characteris-

tics of power sources. Compared to the optimization strategy, RBCS is simple and can be easily applied into the reality, but optimal results are more hardly reached [15].

Optimization based control strategy including local optimization control strategy and global optimization control strategy uses analytical or numerical optimization algorithms to seek for optimal results at a specified sampling time [16, 17]. Global optimization control strategy uses the whole drive cycle as the optimization time and the knowledge about the power demand in sampling time is known in advance. Minimizing cost function is reached through optimal algorithms like dynamic programming [18], genetic algorithmic [19], liner programming [20] and particle swarm programming [21]. High computation cost and relying on road knowledge discourage its on-line usage. Local optimization strategy calculates optimal results in instantaneous time to overcome these problems.

Equivalent consumption minimization strategy (ECMS), as one kind of local optimization strategy, is used for FCHEV to split the power among PEMFC, battery and supercapacitor. The vast majority of research in the literature using ECMS focus on architectures using only two sources. Moreover, literature papers which use the same architecture as the one described in this paper neglect the supercapacitor equivalent hydrogen consumption, which is taken as null [22, 23, 24]. It is not only counter to the aim of minimizing whole hydrogen consumption at every sample time but also increases the complication of EMS, because an additional control strategy is needed to calculate supercapacitor reference power. Therefore, an ECMS calculating whole hydrogen consumption of all three power sources is designed for the FCHEV in this paper and is validated by the experimental test bench [25].

During the lifetime of FCHEV, the power sources degradation appears. As the main power source of FCHEV, the output power of fuel cell at corresponding current decreases along with degradation and its maximum efficiency point of operation also changes. The capacity of battery decreases, and its resistance increases along with its degradation, which decreases the output voltage of battery

[26]. Besides, precise estimation of battery SOC is not possible without considering its degradation. Therefore, fuel cell and battery ageing models are needed to monitor their state of health (SOH) to ensure the performance, safety, availability and reliability of power sources [27]. Supercapacitor lifetime is far larger than the vehicle and its other power sources, so its degradation can be neglected [28]. Then degradation of power sources is defined as fuel cell degradation and battery degradation in the following parts of the paper.

Using control parameters of EMS with healthy power sources into the situation of degraded power sources cannot reach optimal results for EMS and evenly cannot make sure the normal operation of the vehicle [29]. The equivalent factor (EF) of ECMS decides the conversion from electrical energy of ESSs to the equivalent fuel consumption, which can ensure the optimal control solution can be reached with the aim of minimizing the whole fuel consumption [30]. The degradation of power sources also affects the optimal EF value of ECMS and its deviation may even lead to unacceptable operations of the vehicle except for suboptimal results [31]. Therefore, the effects of power sources degradation on ECMS are analyzed in the paper, which is rarely studied by researchers. A novel adaptive ECMS (AECMS) is designed through tuning equivalent factor (EF) based on power sources degradation states. The dynamic power change rate of fuel cell is also adjusted along with power sources degradation to decrease fuel cell degradation rate.The gap between health management of power sources and EMS is filled by integrating the prognostics into the developed AECMS.

This paper is organized as follows: section two describes the vehicle architecture and the model of the powertrain including fuel cell, battery, supercapacitor and DC/DC converters. In the third section, SOH estimation of power sources is explained. In the fourth part, ECMS strategy in the health state is designed and validated through experimental test bench. In the fifth part, the effects of fuel cell degradation and battery degradation on ECMS are analyzed respectively and new AECMS strategy is designed. Finally, conclusions are drawn.

## 2. Vehicle models

### *2.1. Powertrain architecture*

The architecture of FCHEV is shown in Figure 1. Through the reaction between hydrogen and oxygen, PEMFC as the main power source transforms the chemical energy into electric energy and it is connected to DC bus through a unidirectional DC/DC converter. Supercapacitor as the peak power supplier is connected to DC bus via a bidirectional DC/DC converter. Lithium-ion battery as the main energy storage source is directly connected to DC bus to hold the DC bus voltage.

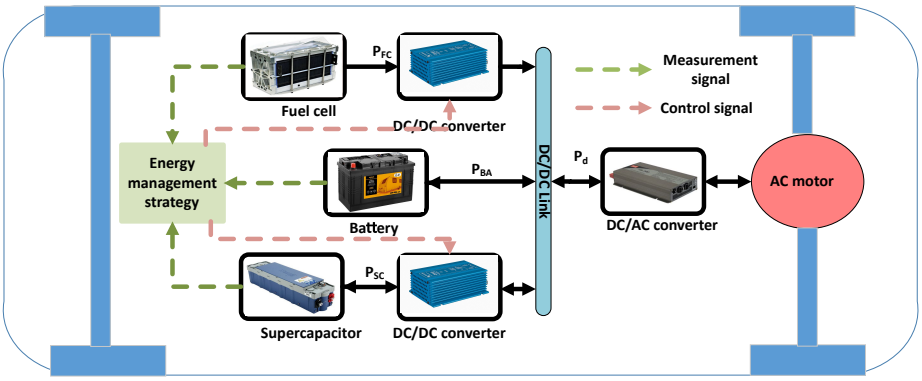


Figure 1: Powertrain architecture

The vehicle propulsion power at wheel can be calculated through the longitudinal dynamics of a road vehicle as equation (1) [32]:

$$P_{cycle}(t) = v\left(m_v(t)\frac{\mathrm{d}}{\mathrm{d}t}v(t) + F_a(t) + F_r(t) + F_g(t)\right) \tag{1}$$

where $P_{cycle}$ is the power demand from drive cycle, $F_r$ the rolling friction, $F_a$ the aerodynamic friction, and $F_g$ the force caused by gravity when driving on slope road:

$$F_a = \frac{1}{2}\,\rho\,A\,C_x\,v^2 \quad (2)$$

$$F_r = m_v\,C_r\,g\,\cos(\alpha) \quad (3)$$

$$F_g = m_v\,g\,\sin(\alpha) \quad (4)$$

where variable $v$ is the speed of the vehicle, $\rho$ is the air density, $m_v$ the vehicle mass, $A$ front surface of the vehicle, $g$ gravitational acceleration, $C_x$ the drag coefficient, $C_r$ the aerodynamic drag coefficient, and $\alpha$ the angle defining the slope of the road.

The power demand $P_{demand}$ on the DC bus should be met by three power sources and its value can be calculated through equation (5).

$$P_{demand} = \frac{P_{cycle}}{\eta_{DC/AC} * \eta_{motor}} \quad (5)$$

where $\eta_{DC/AC}$ is converter efficiency of DC/AC connected to a motor, $\eta_{motor}$ is motor efficiency.

### *2.2. Fuel cell stack model*

1.2 kW PEMFC is chosen as the main power source of FCHEV. The fuel cell stack voltage can be described as equation (6) [33].

$$E = N_{cell} * (E_{rev} - E_{act} - E_{ohm} - E_{con}) \quad (6)$$

where $E_{rev}$ is the thermodynamic reversible potential, $E_{act}$ the activation losses, $E_{ohm}$ the ohmic losses, $E_{con}$ the concentration losses.

The thermodynamic reversible potential can be calculated as equation (7) [34].

$$E_{rev} = E_0 - 0.85e^{-3}(T - T_c) + \frac{RT}{2F} ln(\sqrt{P_{O_2}} P_{H_2}) \quad (7)$$

where $E_0$ is the reversible nearest potential for a single cell, $T$ is the temperature of the cell, $T_c$ is the temperature correction offset, $P_{O_2}$ and $P_{H_2}$ are partial pressure of oxygen and hydrogen.

The dynamic activation losses $E_{act}$ can be described as equation (8).

$$\frac{dE_{act}}{dt} = \frac{I_{FC}}{C_{dl}}\left(1 - \frac{E_{act}}{\eta_{act}}\right) \tag{8}$$

where $C_{dl}$ is the single-fuel cell double-layer capacitance.

The static activation losses $\eta_{act}$ can be simplified as equation (9), when $\eta_{act}$ is large.

$$\eta_{act} = \frac{RT}{2\alpha F} ln\left(\frac{I_{FC}}{I_0}\right) \tag{9}$$

where $I_0$ is the exchange current density, $\alpha$ is the symmetry factor.

The ohmic losses $E_{ohm}$ can be obtained through equation (10).

$$E_{ohm} = I_{FC} * R_{FC} \tag{10}$$

where $R_{FC}$ is the internal resistance.

Concentration losses $E_{con}$ can be calculated as equation (11).

$$E_{con} = -B * ln\left(1 - \frac{I_{FC}}{I_{max}}\right) \tag{11}$$

where B is an empirical constant. $I_{max}$ is the maximum allowed current. According to the above function, the relation between fuel cell voltage and current can be defined.

Fuel cell transforms the chemical energy into electrical energy through the reaction between hydrogen and oxygen [35]. The theoretical efficiency of energy conversion is defined as the ratio between the useful energy output and the energy input. The energy output of fuel cell is the output electrical energy and the energy input is the energy contained in the mass of hydrogen supplied [36]. Besides that, some auxiliary equipment is needed to make sure the normal operation of fuel cell system, like an air compressor, cooling fan and control border. The energy consumed by auxiliary equipment belongs to auxiliary efficiency. The whole fuel cell system efficiency can be defined as equation (12).

$$\eta_{FCS} = \eta_{TH} * \eta_{AUX} = \frac{V_{FC}}{1.254}\left(\frac{P_{FC} - P_{AUX}}{P_{FC}}\right) \tag{12}$$

where $\eta_{TH}$ is the theoretical efficiency, $\eta_{AUX}$ is auxiliary efficiency, $P_{AUX}$ auxiliary power.

The air compressor system and cooling system of fuel cell system are the main auxiliary equipment for this fuel cell system [37], which are built based on the experimental test. Power demand by the compressor is shown as equation (13).

$$P_{cp} = \frac{C_P T_{air}}{\eta_{mec}\eta_{mot}} \left( \left( \frac{P_{out}}{P_{in}} \right)^{\frac{\gamma-1}{\gamma}} - 1 \right) F_{cp} \tag{13}$$

where $P_{cp}$ is air compressor power, $\eta_{mec}$ represents the compressor mechanical efficiency, $C_P$ heat capacity of air, $T_{air}$ inlet air temperature, $\eta_{mot}$ is the efficiency of the compressor motor, $P_{in}$ and $P_{out}$ are input and output air pressures respectively, $\gamma$ is the ratio of the specific heat of air.

$F_{cp}$ is the compressor air flow rate is decided by fuel cell output current as equation (14).

$$F_{cp} = S * M_{air} \frac{N_{cell} * I_{FC}}{4X_{O_2} * F} \tag{14}$$

where $S$ is the stoichiometric ratio, $M_{air}$ is the number of air moles, $X_{O_2}$ oxygen molar fraction.

From the experimental measurement, the speed of controlled cooling fan is divided into a constant speed zone and regulated zone, depending on the stack temperature, as shown in the Table 1 [38].

It should be noticed the DC/DC converter connected to fuel cell system affects the output power of fuel cell system on DC bus. So, its efficiency is also included in fuel cell system. So its efficiency can be calculated as Figure 2.

It can be observed that there is a maximum efficiency point 42.83% at fuel cell current $9.5A$. The high efficiency zone is defined from $4.5A$ to $20A$ in red color, where the value exceeds 40%. In order to reduce the final hydrogen consumption, fuel cell should be operated to seek maximum efficiency point at this zone. When fuel cell requirement is lower than $4.5A$, the fuel cell is turned off to save hydrogen.

Table 1: Cooling fan speed and stack temperature

| **In nonregulated zone** | |
|---|---|
| Stack temperature range | Fan speed (%) |
| to 50.5 ◦C | 35 |
| From 50.5 ◦C to 53.5 ◦C | 36 |
| From 53.5 ◦C to 55.5 ◦C | 37 |
| From 55.5 ◦C to 58.5 ◦C | 38 |
| From 58.5 ◦C to 60.5 ◦C | 39 |
| From 60.5 ◦C to 63.5 ◦C | 40 |
| From 63.5 ◦C to 65.5 ◦C | 41 |
| From 65.5 ◦C to 67.5 ◦C | 42 |
| **In regulated zone** | |
| Fan speed regulator start temperature: 67.5 ◦C | |
| Fan speed regulator stop temperature: 65.0 ◦C | |

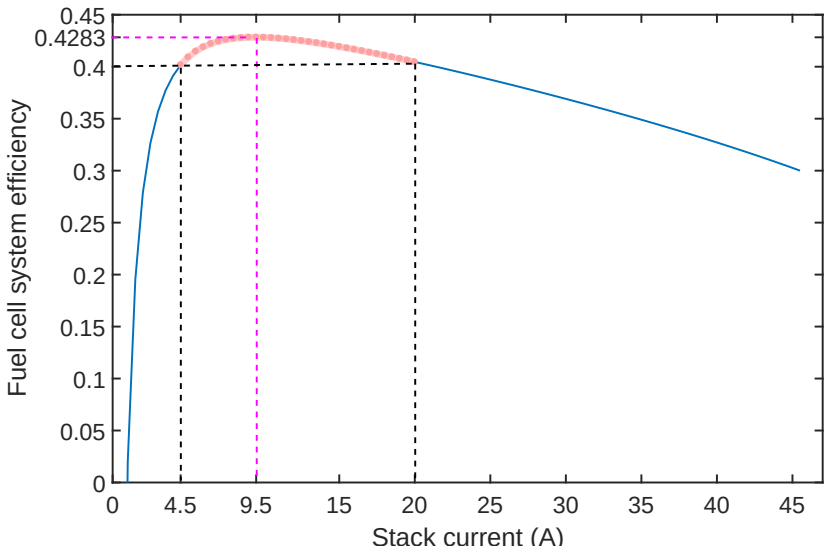


Figure 2: Fuel cell system efficiency curve along with stack current

The hydrogen consumption rate can be defined by fuel cell current as the following equation (15) [39]:

$$m_{H2} = \int_0^t \frac{M_{H_2} N_{cell}}{2\,F} I_{FC}(t)\,dt \tag{15}$$

where $m_{H_2}$ is the hydrogen mass rate, $M_{H_2}$ the hydrogen molar mass.

*2.3. Battery model*

An electrochemistry-based Lithium-ion battery model is used in this paper. Compared to the empirical model, multi-physical model and equivalent circuit battery model, the new model not only can make sure the low cost of computation but also meets the high accuracy requirement [40].

Li-ion battery is composed of a positive electrode, a negative electrode and an electrolyte. During discharge, lithium ions ($Li^+$) de-insert from the negative electrode consisting of lithiated carbon($Li_xC$), diffuse through the separator consisting of electrolyte towards the positive electrode and intercalate in the positive electrode consisting of lithium cobalt oxide ($Li_xCoO_2$) [41]. The charging process is the reverse of discharging process. The voltage terms of the battery are summarized in Figure 3. The overall voltage of battery $V(t)$ is the difference between the positive current collector potential and negative current collector potential, and resistance losses at the current collectors are taken as zero [42]. According to Figure 3, the battery voltage can be expressed as the equation (16)

$$V\,(t) = V_{U,p} - V_{U,n} - V_{S,p} - V_{S,n} - V_e - V_{O,n} - V_{O,p} \tag{16}$$

where $V_{U,p}$, $V_{U,n}$ are equilibrium potentials at the positive current collector and the negative current collector respectively, $V_{O,n}$ and $V_{O,p}$ are surface overpotentials due to charge transfer resistance at the positive and negative current collector, $V_{S,p}$ $V_{S,n}$ and $V_e$ are the voltage drop due to solid phase ohmic resistance at the positive and negative current collector and the electrolyte ohmic resistance respectively. Each of these voltages is described in detail in the following parts.

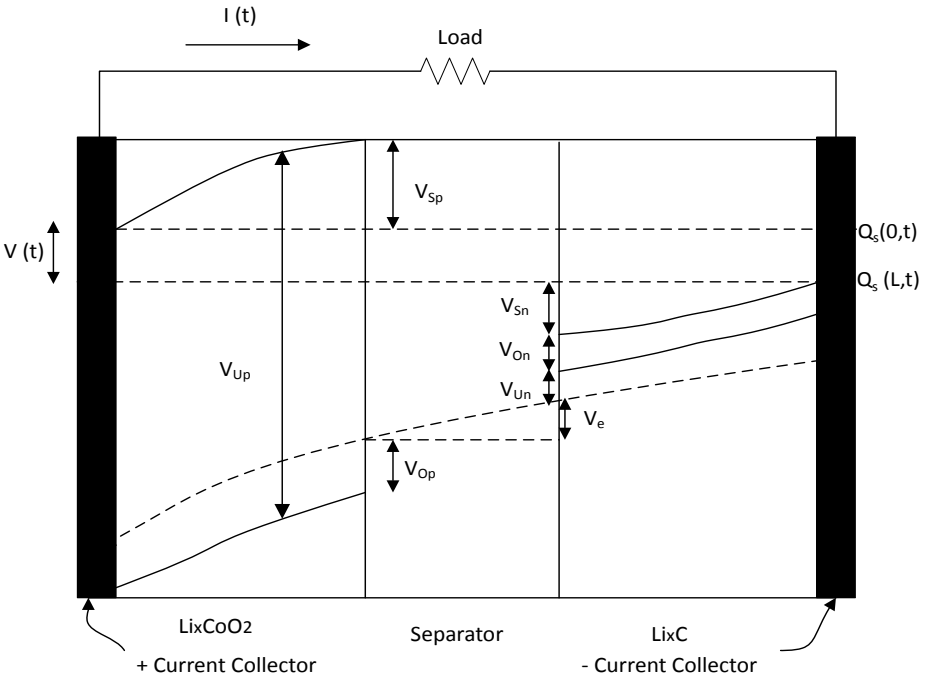


Figure 3: Battery model

Equilibrium potential can be calculated as the Nernst equation (17):

$$V_{U,i} = U_0 + \frac{RT}{nF} ln\left(\frac{1-x_i}{x_i}\right) + V_{act,i} \tag{17}$$

where $i$ stands for the electrode ( $n$ for negative and $p$ for positive), $U_0$ is reference voltage, $T$ is electrode temperature, $n$ the number of electrons transferred in the reaction, $V_{act,i}$ the activity correction term (0 in the ideal condition), which can be defined as equation (18) [43].

$$V_{act,i} = \frac{1}{nF}\left(\sum_{k=0}^{N_i} A_{i,k}\left((2x_i-1)^{k+1} - \frac{2x_i k\,(1-x_i)}{(2x_i-1)^{1-k}}\right)\right) \tag{18}$$

$x_i$ can be defined as equation (19).

$$x_i = \frac{q_i}{q_{max}} \tag{19}$$

where $q_i$ the amount of Li ions in electrode i, $q_{max} = q_p + q_n$, the total amount of Li ions. $x_p + x_n = 1$, when fully charged $x_p = 0.4$ and $x_n = 0.6$. When fully discharged, $x_p = 1$ and $x_n = 0$.

The equilibrium voltage is directly decided by the amount of charge in the electrodes. Each electrode can be divided into surface layer (subscript s) and buck layer (subscript b). So the relationship can be determined by:

$$q_p = q_{s,p} + q_{b,p} \tag{20}$$

$$q_n = q_{s,n} + q_{b,n} \tag{21}$$

$$q_{max} = q_{s,n} + q_{b,n} + q_{s,p} + q_{b,p} \tag{22}$$

In the buck layer, the concentration of Li ion is nearly even but inside the surface layer, the concentration changes drastically. The concentrations of Li ions in the surface layers are described as:

$$c_{b,i} = \frac{q_{b,i}}{v_{b,i}} \tag{23}$$

$$c_{s,i} = \frac{q_{s,i}}{v_{s,i}} \tag{24}$$

where $q_{s,i}$ and $q_{b,i}$ are the charge at different layers, $v_{b,i}$ and $v_{s,i}$ are the volume of layers. The diffusion rate from the bulk to the surface is:

$$q_{bs,i}{}' = \frac{c_{b,i} - c_{s,i}}{D} \tag{25}$$

Where D is the diffusion constant. So the charge variables are calculated as:

$$\begin{aligned} q_{s,p}{}' &= i_{app} + q_{bs,p}{}' && (26)\\ q_{b,p}{}' &= i_{app} + q_{bs,p}{}' - i_{app} && (27)\\ q_{b,n}{}' &= i_{app} + q_{bs,n}{}' - i_{app} && (28)\\ q_{s,n}{}' &= -i_{app} + q_{bs,n}{}' && (29) \end{aligned}$$

where $i_{app}$ is the applied electric current, the mole fraction in the surface and buck can be calculated based on the charge:

$$\begin{aligned} x_i &= \frac{q_i}{q_{max}} && (30)\\ x_{s,i} &= \frac{q_{s,i}}{q_{s,i,max}} && (31)\\ x_{n,i} &= \frac{q_{n,i}}{q_{n,i,max}} && (32) \end{aligned}$$

According to above function the value of $V_{U,p}$ and $V_{U,n}$ can be calculated. Regarding $V_{S,p}$, $V_{S,n}$, $V_e$, they can be categories as the Ohmic potential:

$$\begin{aligned} V_r &= V_{S,p} + V_{S,n} + V_e \\ &= i_{app}\left(R_{S,p} + R_{S,n} + R_e\right) \\ &= i_{app} R \end{aligned} \tag{33}$$

The surface potentials $V_{O,n}$ and $V_{O,p}$ are due to charge transfer resistance and solid-electrolyte interface (SEI) kinetics can be calculated as the simplified Butler-Volmer equation (34).

$$V_{O,i} = \frac{RT}{F\alpha} arcsin\left(\frac{J_i}{2J_{i0}}\right) \tag{34}$$

where $\alpha$ is the symmetry factor, $J_i$ is the current density, $J_{i0}$ is the exchange current density.

Now that, all potentials at equation (16) are defined. Regarding the battery dynamic changes can be calculated as:

$$V(t) = V_{U,p} - V_{U,n} - V_r{}' - V_{O,n}{}' - V_{O,p}{}' \quad (35)$$

$$V_r{}'' = \frac{V_r - V_r{}'}{\tau_r} \quad (36)$$

$$V_{o,i}{}'' = \frac{V_{o,i} - V_{o,i}{}'}{\tau_{o,i}} \quad (37)$$

where $\tau$ are empirical time constants.

The SOC of the battery can be calculated according to the charge on the buck and surface layer and the whole amount of charge, scaled from 0 to 1 as equation (38).

$$SOC = \frac{q_n}{0.6 q_{max}} \quad (38)$$

*2.4. Supercapacitor model*

The equivalent circuit model of the supercapacitor is simplified into an equivalent capacitor connected with a resistor in series [44]. The capacitor accounts for the canonical capacitance effect of supercapacitor, while the series resistor represents the overall ohmic losses [45]. Compared to rechargeable battery, supercapacitor has unique electrostatic energy storage characteristic that the supercapacitor SOC is directly related to its terminal voltage, so its SOC and output current can be calculated through equation (39)(40).

$$SOC = \frac{V_{max} - V_t}{V_{max} - V_{min}} \quad (39)$$

$$I = \frac{V_{oc} - \sqrt{V_{oc}^2 - 4RP})}{2R} \quad (40)$$

where $V_{max}$ is maximum output voltage, $V_{min}$ output minimum voltage, $V_t$ is voltage at sample time t, $R$ equivalent resistance, $P$ the output power of supercapacitor.

*2.5. DC/DC converter model*

As described in Section 2.1, a DC/DC boost converter and a DC/DC buck/boost converter are connected to the fuel cell and supercapacitor respectively. Each converter has two IGBT transistors controlled by two complementary pulse width modulation (PWM) signals which are calculated according to fuel cell and supercapacitor reference currents as Figure 4. The same topology is applied to design the DC/DC converter between fuel cell and DC-bus. Nevertheless, in this case, only one IGBT transistor is used (s2), the other one is always set to off mode.

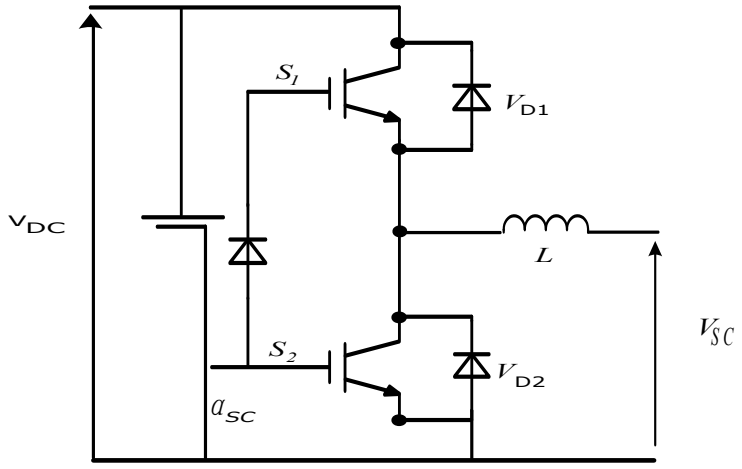


Figure 4: 2-quadrant DC/DC buck/boost converter for supercapacitor

The relationship between input power and output power of two converters is shown as equation (41).

$$I_{out} = \eta_{conv} \frac{P_{in}}{U_{out}} \tag{41}$$

where $P_{in}$ is input power, $U_{out}$ is output voltage and $\eta_{conv}$ is DC/DC converter efficiency.

## 3. Estimation of power sources SOHs

The degradation of power sources affects the normal operation of EMS. In this section, the method used to determine both fuel cell and battery SOHs is presented. Model based prognostic approach is used to asses the power sources degradation. The main advantage of using this method is the small amount of data required and its on-line implementation ability. Joint state parameter estimation is the main prognostic problem in this paper and the health of power sources is determined based on the estimated state parameters [46]. The prognostic model has strong non-linearity, so a non-linear filter is required. The unscented Kalman filter (UKF) has not only higher accuracy than extended Kalman filter but also lower computational cost than particle filter [47]. Therefore in this paper, UKF is chosen to estimate the battery SOH and fuel cell SOH. The basic framework for the UKF estimation of the state of a discrete-time non-linear dynamic system as following equations [48]:

$$x_{k+1} = F(x_k, u_k, v_k) \tag{42}$$

$$y_k = H(x_k, n_k) \tag{43}$$

where $x_k$ is the unobserved state of the system, $u_k$ is the input, $v_k$ is the process noise, $y_k$ is the observed measurement signal, $n_k$ the observed noise.

The general architecture of the prognostic approach to estimate fuel cell and battery SOHs using UKF is shown in Figure 5 [49]. Through the input reference currents of fuel cell and battery ($u_k$) and the real output voltages ($y_k$) measured by sensors, UKF is used to estimate and modify the unobserved state parameters ($x_k$) of their degradation model. With the right estimated state parameters, their SOHs can be determined.

### *3.1. Battery degradation and on-line state of health estimation*

As described in section 2.3, battery model parameters $q_{s,n}$, $q_{b,n}$, $q_{s,p}$, $q_{b,p}$, ${V_{o,p}}'$, ${V_{o,n}}'$, ${V_r}'$ are taken as states variables $x$, and battery output voltage $V$ as the output variable $y$. In order to save time and reduce computational cost,

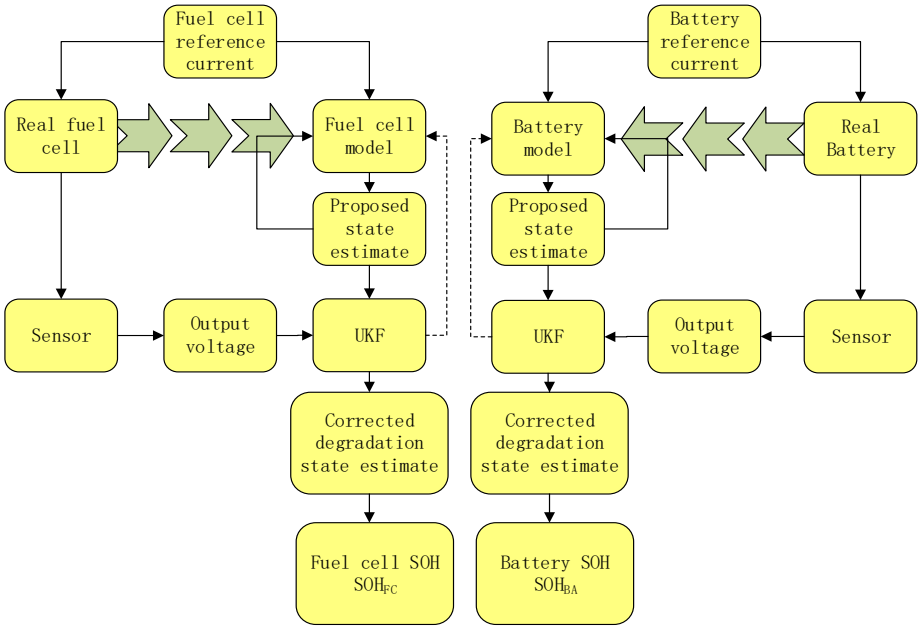


Figure 5: The general architecture of prognostic approach for estimation of power sources SOHs

one single battery is tested under a random sequence of charging (negative) and discharging (positive) currents among (-4.5A, -3.75A, -3A, -2.25A, -1.5A, -0.75A, 0.75A, 1.5A, 2.25A, 3A, 3.75A, 4.5A) [50]. This type of charging and discharging operation is referred to here as a random walk (RW) operation. The fitting results of battery model under several RWs are shown as Figure 6

It can be observed that the battery model can well fit the measurement of battery in the health state. Along with battery degradation, some physical ageing phenomena can be observed such as SEI layer growth, lithium corrosion, lithium loss of lithium plating and changes in diffusion property [51]. The fitting result of the same battery model under health state for an aged battery can be seen in Figure 7.

It can be observed that the error between estimated battery voltage through the model and real measured voltage is large. So some parameters of battery model should be changed along with battery ageing. For the electro-chemistry

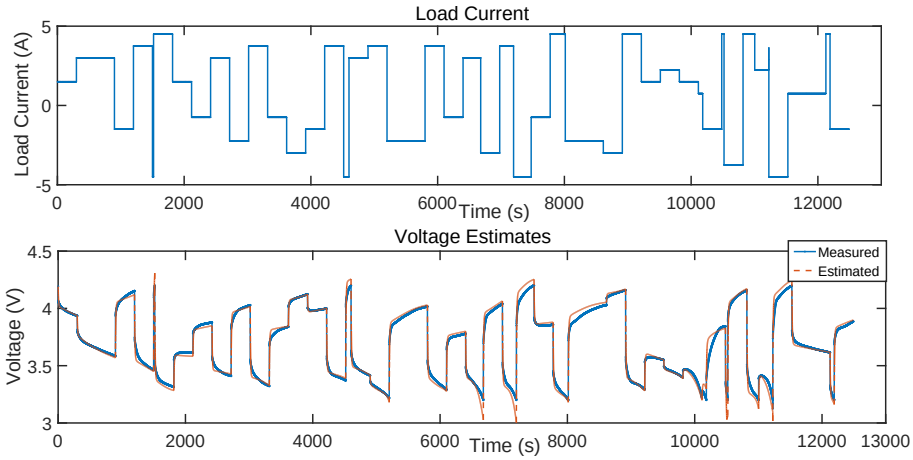


Figure 6: Battery model fitting for new battery

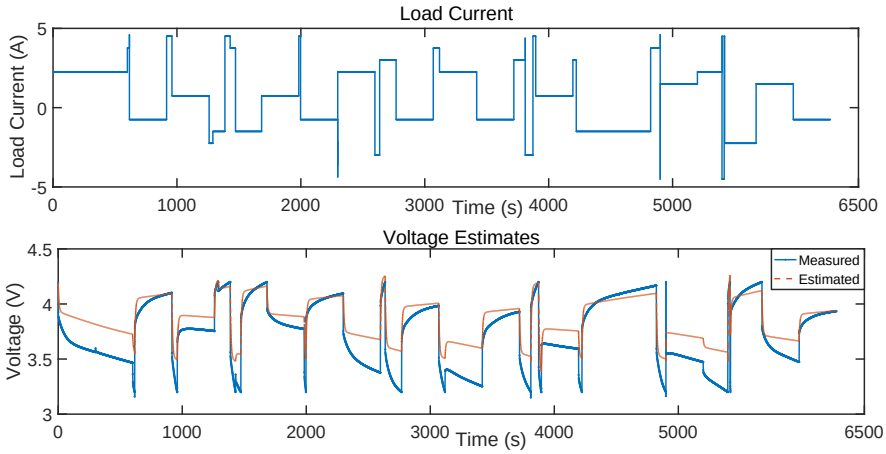


Figure 7: Battery model fit for aged battery

based model, the maximum charge $q_{max}$, which stands for the loss of active Li ions due to degradation, the internal resistance $R$ representing SEI layer growth and the diffusion constant $D$ are selected as the ageing parameters of battery ageing mode. Along with the degradation, $q_{max}$ decreases, $R$ and $D$ increase. The state of health of battery can be calculated based on $q_{max}$, as equation (44).

$$SOH_{BA} = \frac{q_{max}^{int} - q\left(t\right)}{q_{max}^{int} - q_{max}^{min}} \tag{44}$$

where $q_{max}^{int}$ battery initial maximum charge, $q_{max}^{min}$ is the 50% of the $q_{max}^{int}$, which is the threshold of battery end of life, $q\left(t\right)$ is battery maximum charge at time t.

The ageing parameters ($q_{max}$, $R$, $D$) change in time as a function of usage. The dynamic change rate can be described as:

$$q_{max}{}' = w_q \left|i_{app}\right| \tag{45}$$

$$R' = w_R \left|i_{app}\right| \tag{46}$$

$$D' = w_D \left|i_{app}\right| \tag{47}$$

where $i_{app}$ is the applied current, $w_q$, $w_R$ and $w_D$ are the ageing rate parameters.

The experimental test of random charge/discharge sequences of battery can well simulate battery operations in the vehicle due to its randomness. Therefore, a 3140 minutes experimental test data is used to verify the validation of battery degradation model. The modification of battery degradation parameters is determined by UKF based on the on-line measured battery voltages from the 3140 minutes experiment test. The measured and estimated battery voltages, estimated degradation parameters $q_{max}$ and its SOH along with time are shown in Figure 8 and Figure 9.

With the added degradation state parameters, the battery voltage estimated by UKF and its degradation model can match well with the measured volt-

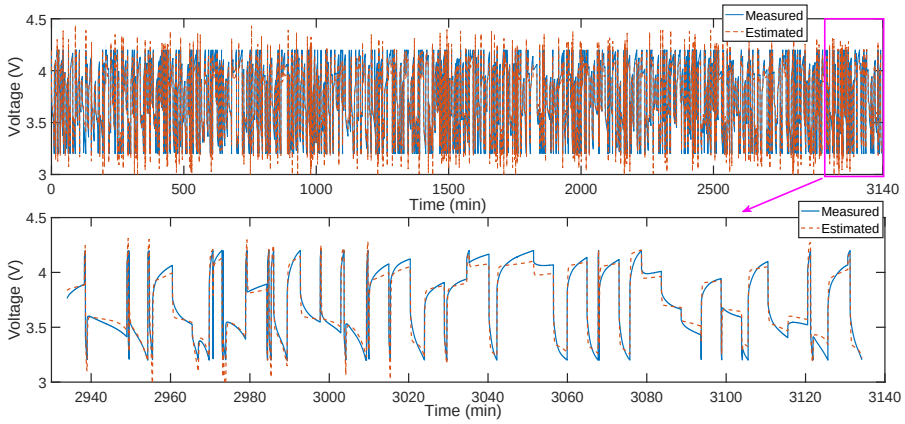


Figure 8: Battery degradation model fit for aged battery

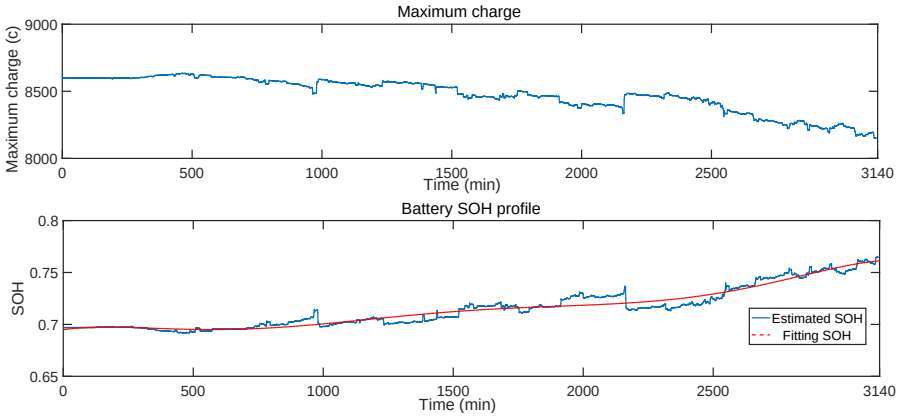


Figure 9: On-line UKF estimates of the degradation state parameter and SOH

age over the random charge/discharge sequences. Some errors are still present which are due to temperature effects. The internal battery temperature changes over time are not considered in the degradation model. The change of battery charge/discharge currents leads to the variation of battery degradation state, which results in the fluctuation of the decreasing trend of $q_{max}$ in Figure 9. According to the estimated $q_{max}$ value, battery SOH can be calculated through equation (44) and its range is (0,1). Even though there are some fluctuations of SOH, the whole trend of battery, which is shown as the line in red color, increases along with time meaning the increase of battery degradation. Meanwhile, the battery SOC also can be precisely estimated with decreasing $q_{max}$ along with time based on equation (38).

### *3.2. Fuel cell degradation and on-line state of health estimation*

Upon long term operation of PEMFC, its main components including membrane, electrodes, bipolar plates, gas diffusion layers, and sealing gaskets would undergo mechanical, chemical and electrochemical degradation changes resulting in the decrease of fuel cell performance [52]. The presented fuel cell degradation model is designed based on the fuel cell model of Section 2.2. The sample time of fuel cell ageing process is much larger than the one of fuel cell dynamic model. So all the dynamic changes of fuel cell are neglected. The static voltage of the PEMFC can be described as equation (48) [53].

$$E = N_{cell} * \left( E_{rev} - A * ln\left(\frac{I_{FC}}{I_0}\right) - R * I_{FC} - B * ln\left(1 - \frac{I_{FC}}{I_{max}}\right)\right) \quad (48)$$

According to the previous study of [54, 55], the resistance $R$ and maximum current $I_{max}$ have large variations along with fuel cell degradation, which are chosen as the degradation state parameters. Their variations with time can be described as [56]:

$$R(t) = R_0(1+\alpha(t)) \quad (49)$$

$$I_{max}(t) = I_{max0}(1-\alpha(t)) \quad (50)$$

$$\alpha(t) = \beta * t \quad (51)$$

where $R_0$ and $I_{max0}$ are the initial values, $\alpha$ and $\beta$ represent degradation variance and degradation rate along with time. The fuel cell SOH can be defined as equation (52).

$$SOH_{FC} = \frac{\alpha(t) - \alpha_{min}}{\alpha_{max} - \alpha_{min}} \quad (52)$$

The estimation of $SOH_{FC}$ relies on the precise estimation of $\alpha$ and $\beta$ through the following discrete non-linear system as equation (53), (54).

$$x_{k+1} = A * x_k + w_k \quad (53)$$

$$y_k = g(x_k, u_k) + v_k \quad (54)$$

where $x_k = [\alpha, \beta]^T$ is the UKF state variable, $A = [1, T; 0, 1]$, $y_k$ is the fuel cell voltage, $w_k$ and $v_k$ are process and observation noises, $u_k$ is the input current load, $g(x_k, u_k)$ is described as (48).

In order to verify the validation of fuel cell degradation model, a PEMFC experimental degradation voltage data is used, which are achieved through a 400 h experimental degradation test on a 1.2 kW commercial Ballard NEXA PEM fuel cell stack [57]. The fuel cell output current is kept as 12A for the whole experimental period. Fuel cell degradation model is used to estimate the fuel cell voltage along with the experimental test. The variation of degradation parameters of fuel cell degradation model is determined by UKF based on the on-line measured fuel cell voltage through voltage sensor. The measured and estimated fuel cell voltages, estimated degradation parameters $\alpha$ and its SOH along with time are shown in Figure 10.

It can be observed from Figure 10, the estimated fuel cell voltages through UKF accurately fit with the measured voltages from the experimental data,

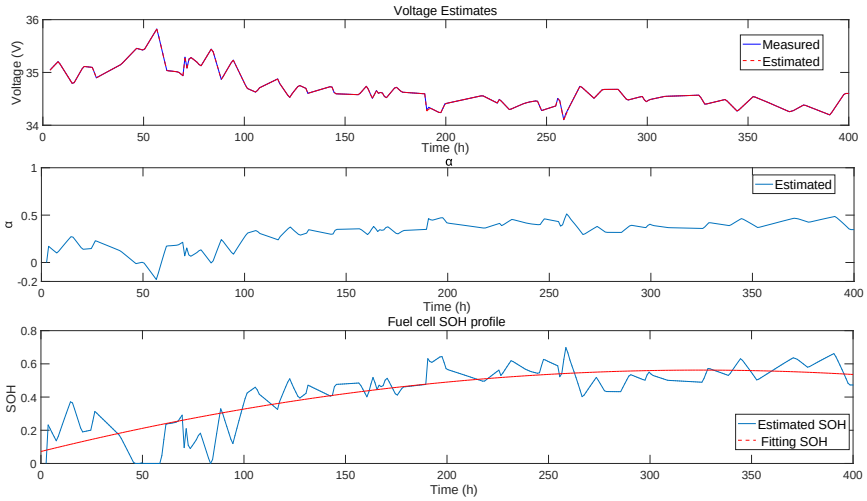


Figure 10: Estimation of the stack voltage, degradation parameter $\alpha$ and SOH

which can prove the accuracy of the online estimation model. The negative degradation parameter $\alpha$ and its fluctuations are due to the reversal of fuel cell degradation. When $\alpha$ is less than 0, its value is set as zero. With the estimated value of $\alpha$, the fuel cell SOH can be calculated through equation (52) and its range is (0,1). It also can be observed that the general trend of fuel cell SOH in red color increases along with time.

## 4. Energy management strategy

### *4.1. Equivalent consumption minimization strategy*

In order to minimize hydrogen consumption and prolong the fuel cell lifetime, an ECMS is designed. The core idea of ECMS is transforming the electric consumption from battery and supercapacitor into equivalent hydrogen consumption and minimizing the sum of the equivalent hydrogen consumption and direct hydrogen consumption from fuel cell [58]. Meanwhile, some constraints are added to make sure the normal operation of power sources. Its optimal equation can be described as the following equation (55):

$$
\begin{aligned}
&min\ f_w(t) = m_{FC}(t) + m_{BA}(t) + m_{SC}(t) \\
&\begin{cases}
I_{FC}^{min} \le I_{FC} \le I_{FC}^{max} \\
I_{SC}^{min} \le I_{SC} \le I_{SC}^{max} \\
-dI_{FC} \le \frac{I_{FC}(t) - I_{FC}(t-1)}{T} \le dI_{FC}
\end{cases}
\end{aligned} \tag{55}
$$

where $f_w(t)$ represents whole hydrogen consumption at sample time $t$, $m_{FC}(t)$ is fuel cell hydrogen consumption, $m_{BA}(t)$ is battery equivalent hydrogen consumption, $m_{SC}(t)$ represents supercapacitor equivalent hydrogen consumption, $I_{FC}$ and $I_{SC}$ represents the current of fuel cell and supercapacitor respectively, $I_{SC}^{min}$ is minimum current (-18A), $I_{SC}^{max}$ are maximum current (18A), $I_{FC}(t)$ and $I_{FC}(t-1)$ is fuel cell current at time t and at time t-1, $dI_{FC}$ is fuel cell maximum current change rate (1A/S). In case fuel cell works at low efficiency zone at very low current and frequent on/off cycle, the minimum current of fuel cell $I_{FC}^{min}$ is set as 4.5A, less than that value, fuel cell is shut off. The maximum current $I_{FC}^{max}$ is its normal current (47A).

In order to let fuel cell seek for its maximum efficiency point in its high efficiency zone and keep charge sustenance of ESSs which means that let the terminal battery and supercapacitor SOC be equal or close to their initial values, some corresponding penalty coefficients are added into the objective function of equation (55) as shown in equation (56).

$$
\begin{aligned}
f_w(t) &= K_{FC} m_{FC}(t) + K_{BA} m_{BA}(t) + K_{SC} m_{SC}(t) \\
&= K_{FC} m_{FC}(t) + K_{BA} \lambda_{BA} P_{BA}(t) + K_{SC} \lambda_{SC} P_{SC}(t)
\end{aligned} \tag{56}
$$

where $K_{BA}$ and $K_{SC}$ are penalty coefficients which limit battery and supercapacitor SOC range and variation between final SOC and initial SOC, $K_{FC}$ is the fuel cell efficiency penalty coefficient, $\lambda_{BA}$ and $\lambda_{SC}$ are the corresponding equivalent factors, $P_{BA}(t)$ and $P_{SC}(t)$ are the battery power and supercapacitor power.

Fuel cell efficiency penalty coefficient $K_{FC}$ is described as equation (57):

$$K_{FC} = \begin{cases} (1 - 2 * \frac{\eta - \eta_{opt}}{\eta_{max} - \eta_{min}})^2 & \eta \geq 0.4 \\ \\ (1 - 2 * \frac{\eta - \eta_{opt}}{\eta_{max} - \eta_{min}})^4 & \eta < 0.4 \end{cases} \tag{57}$$

where $\eta$ is the instantaneous efficiency, $\eta_{opt}$ is optimal efficiency (0.4283), $\eta_{max}$ the maximum efficiency (0.4283), $\eta_{min}$ the minimum efficiency (0). When fuel cell system efficiency is below than 0.4, a large penalty value $K_{FC}$ is calculated to shut fuel cell down or operate fuel cell to meet power demand by drive cycle based on battery and supercpacitor SOC values. The orders of $K_{FC}$ for two conditions are 2 and 4 respectively which are decided by drive cycle power demand. Seeking maximum efficiency point and restricting high efficiency zone ( efficiency above 0.4 ) are controlled through $K_{FC}$.

Battery SOC penalty coefficient $K_{BA}$ is defined as equation (58):

$$K_{BA} = \begin{cases} (1 - \frac{2*(u - B_{int})}{B_{max} - B_{min}})^4 & \mathrm{B}_{min} \leq u \leq B_{max} \\ \\ (1 - \frac{2*(u - B_{int})}{B_{max} - B_{min}})^{20} & \mathrm{u} < B_{min}, u > B_{max} \end{cases} \tag{58}$$

where $u$ is the instantaneous battery SOC, $B_{int}$ is battery initial SOC, $B_{max}$ the maximum SOC, $B_{min}$ the minimum SOC. $K_{BA}$ operates the battery SOC to return back to its initial SOC. When battery SOC reaches $B_{min}$ or $B_{max}$, high $K_{BA}$ value is defined as the punish factor to avoid the battery continues to discharge and charge respectively.

Supercapacitor penalty coefficient $K_{SC}$ is composed of SOC coefficient $S_{eff}$ and peak power coefficient $S_{peak}$. $S_{eff}$ is similar to $K_{BA}$ to limit supercapacitor SOC value at reasonable range. $S_{peak}$ is used to let supercapacitor supply peak power. In order to avoid the frequent fuel cell on/off cycles and frequent supercapacitor charge/discharge cycles due to supercapacitor SOC large amplitude changes in short time, supercapacitor SOC is equivalent to battery SOC

to define $S_{eff}$. $K_{SC}$, $S_{eff}$ and $S_{peak}$ can be defined as following equations respectively:

$$K_{SC} = S_{eff} * S_{peak} \tag{59}$$

$$S_{eff} = \begin{cases} (1 - 2\frac{ax+b-S_{opt}}{S_{max}-S_{min}})^2 & \mathrm{S}_{min} \leq x \leq S_{max} \\ \\ (1 - 2\frac{ax+b-S_{opt}}{S_{max}-S_{min}})^{20} & \mathrm{x} < S_{min}, x > S_{max} \end{cases} \tag{60}$$

$$S_{peak} = \begin{cases} 1 & 0 \leq I_{load} \leq 30 \\ -0.01 * I_{load} + 1 & \mathrm{I}_{load} < 0, I_{load} > 30 \end{cases} \tag{61}$$

where $x$ is the instantaneous supercapacitor SOC, $S_{opt}$ is optimal SOC, $S_{max}$ the maximum SOC, $S_{min}$ the minimum SOC, $I_{load}$ is current demand on the DC bus, $a$ and $b$ are the transform coefficients from supercapacitor SOC to equivalent battery SOC and their values are decided by battery minimum SOC and maximum SOC.

After defining all the parameters in the equation (55), the ECMS strategy is transformed into a nonlinear constrained optimization problem. If this strategy can be used online is decided by computation cost and storage memory requirement. In this paper, sequential based programming (SQP) approach is programmed in C language to solve this problem. The SQP method generates steps by solving quadratic subproblems and it can be used both in line search and trust-region frameworks [59]. The SQP algorithm belongs to a local optimization algorithm that is very useful for solving problems with significant nonlinearities [60].

### *4.2. Experiment implementation and validation*

In order to verify experimentally and evaluate the performances of EMS, a test bench is designed. It includes the main components described at Section 2 such as PEMFC, battery, supercapacitor, DC/DC converters and some other equipment like measurement sensors, power supply, electric load, MicroAutoBox

436 and PC. The parameters of the vehicle and components in the test bench are shown in Table 2.

Table 2: The parameters of the vehicle and components in the test bench

| | | | | |
|---|---|---|---|---|
| Vehicle | Mass | 530 kg | Front surface | 2.56 $m^2$ |
| | Drag coefficient | 0.8 | Rolling coefficient | 0.02 |
| PEMFC | Manufacturer | The Ballard NEXATM | Rated power | 1200 W |
| | Rated current | 46 A | Rated voltage | 26 V |
| | Voltage range | 22-50 V | | |
| Battery | Manufacturer | Yuasa Battery | Capacity | 90 Ah |
| | Numbers | 4 series | Nominal Voltage | 12 V |
| Supercapacitor | Manufacturer | Maxwell Technologies | Rated Capacitance | 58 F |
| | Numbers | 2 series*2 parallel | Rated Voltage | 16 V |
| Experiment conditions | Ambient temperature | 25.18 °C | Input hydrogen pressure | 10.24 Barg |

437

438 Some sensors are used to measure relevant current and voltage values of
439 power sources. The vehicle used in this paper is a light duty vehicle and is
440 designed for the postal delivery service in the university campus or city com-
441 munities. A postal delivery mission is based on a lot of start/stop sequences,
442 making the mean value of speed over time very small. In order to reproduce
443 the behavior of such application, WVUCITY drive cycle, New York Bus drive
444 cycle and LA92 drive cycle are chosen for simulation purposes due to their sim-
445 ilarities with the required average speed and start/stop numbers. Power supply
446 and electric load are used to supply negative power and positive power of drive

cycle respectively. MicroAutoBox Π from dSPACE serves as the control unit. The ECMS is downloaded into this control unit. According to all gathered control signals needed by EMS, the fuel cell reference current and supercapacitor reference current are calculated respectively by the control unit. Two classical PI controllers are applied to adjust duty cycles of PWM signals to control the fuel cell and supercapacitor output currents to track the reference currents as Figure 11. Afterward, 20KHz PWM signal produced by MicroAutoBox Π is transmitted into DC/DC converter and controls its normal operation.

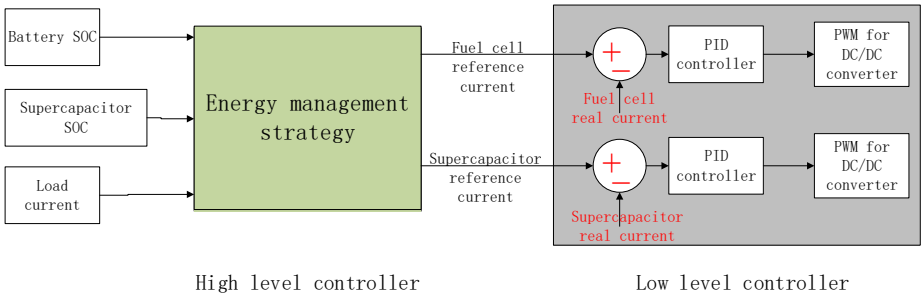


Figure 11: Control system of testbench

Human machine interface in the personal computer is designed under the software ControlDesk 4.2 to monitor the predefined variable's instantaneous value, tune control parameters of the whole control system and record all real time variable's value in order to analyze the final experiment results. The architecture of the test bench is shown in Figure 12.

The experiment and simulation results are shown in Figure 13 including currents of three power sources, SOCs of two energy storage sources as well as fuel cell efficiency penalty coefficient $K_{FC}$, battery SOC penalty coefficient $K_{BA}$ and supercapacitor penalty coefficient $K_{SC}$. In order to facilitate the explanation of the operation process of ECMS strategy, the magnifying simulation results: currents of three power sources and their corresponding penalty coefficients from time 500s to 700s are shown in Figure 14.

It can be observed from Figure 13 that the load currents supplied by a power supply and an electrical load fit well with the simulation current profile

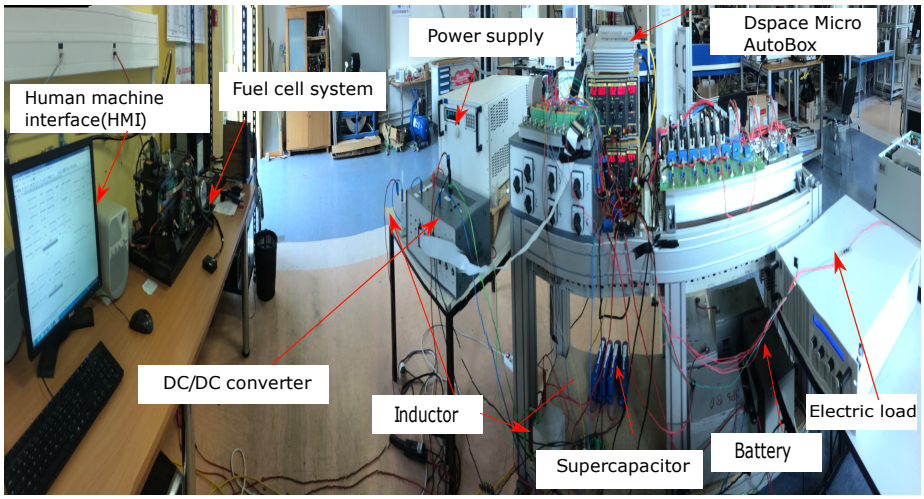


Figure 12: Test bench architecture

of the drive cycle. Fuel cell starts at 440s and 456s for simulation results and experimental results, respectively. Experiment results of fuel cell current and battery current are similar to simulation results. The final simulation result of battery SOC is 0.792 similar to the experiment value 0.7915. Supercapacitor current is sensitive to the power requirement of the drive cycle, fuel cell current and battery SOC, which explains the difference between simulation and experimental results on supercapacitor current. Considering the low energy density of supercapacitor and its role as peak power supplier, this difference can be neglected.

In Figure 14, battery SOC is 0.7967 at simulation time 500s. With the discharge of the battery, its penalty coefficient $K_{BA}$ increases. The objective function of ECMS leads to decrease the battery current to prevent the reduction of battery SOC when the SQP algorithm solves the minimizing objective function of the following step. Fuel cell plays a bigger role in supplying power requirement of drive cycle along with the increase of $K_{BA}$. Meanwhile, its efficiency decreases and $K_{FC}$ decreases along with the increase of its current. Therefore, the difference between the actual current and the maximum efficient one (9.5 A) is enlarged. $K_{FC}$ as a penalty coefficients increases to operate fuel

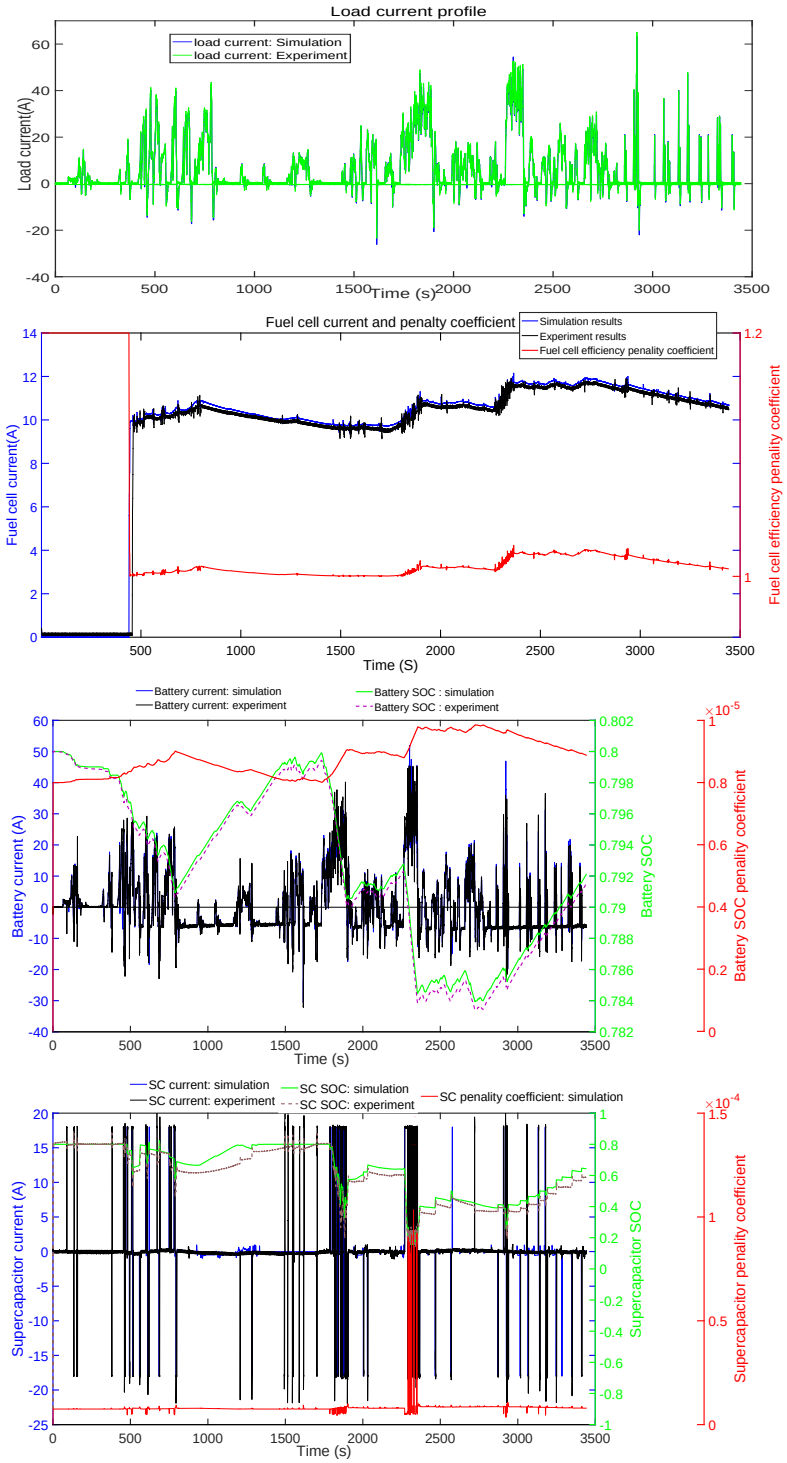


Figure 13: Comparative results between experiment and simulation

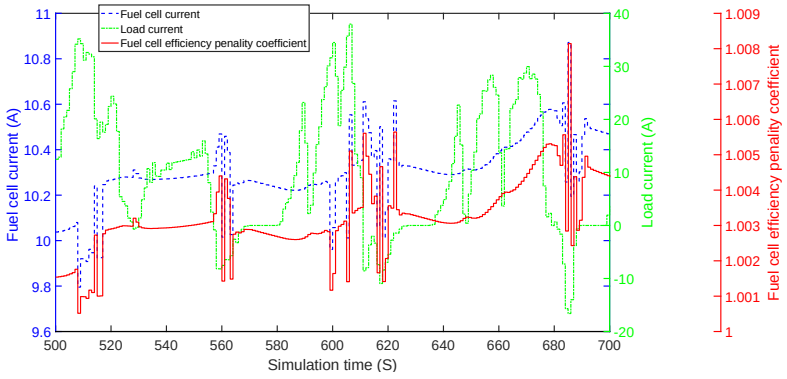


(a) Fuel cell current, load current and penalty coefficient

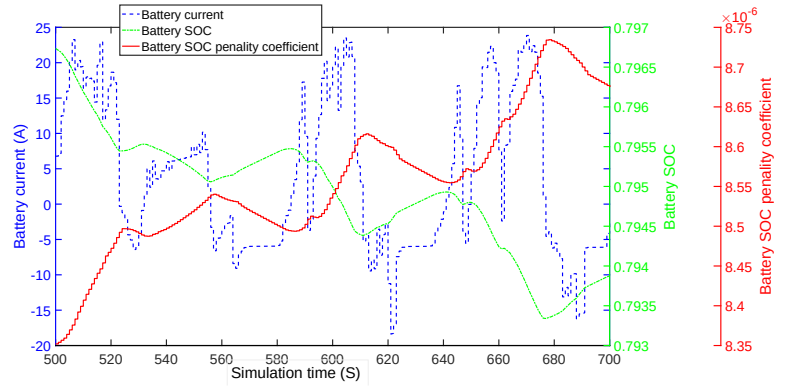


(b) Battery current, battery SOC and battery penalty coefficient

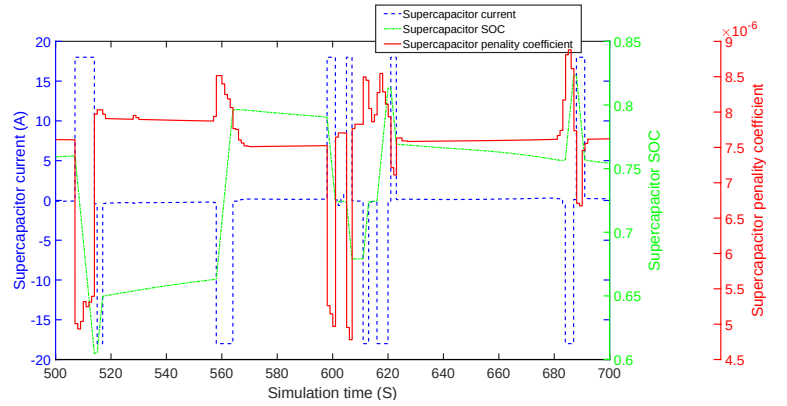


(c) Supercapacitor current, supercapacitor SOC and supercapacitor penalty coefficient

Figure 14: Operations of three power sources

cell to seek for maximum efficiency point. When $K_{BA}$ and $K_{FC}$ both increase to decrease battery current and fuel cell current, their reductions rely on the increasing degree of their penalty coefficients in the objective function. It should be mentioned that the output currents of fuel cell and battery on DC bus should be equal to the load current, which may increase both currents even though $K_{FC}$ and $K_{BA}$ both increase. Supercapacitor is operated as the battery. The only difference is peak power coefficient $S_{peak}$. When the load current is larger than 30A or lower than 0A, $S_{peak}$ is lower than 1 and supercapacitor penalty coefficient $K_{SC}$ gets smaller than battery penalty coefficient $K_{BA}$, leading to discharging firstly in larger current than 30A and charging firstly when the load current is negative.

In order to prove the superiority of the new designed ECMS, A RBCS is designed and it is divided into two parts: load following control strategy (LFCS) as the first part to decide fuel cell reference current, and, operating mode control strategy (OMCS) as the second part to calculate supercapacitor current. Regarding LFCS, fuel cell is set to work in high efficiency zone and its reference current is decided by the current demand of drive cycle and battery SOC value as equation (62). The on/off cycle of fuel cell is also controlled by the LFCS through the added control parameters: fuel cell minimum off time, which means since the fuel cell was last on, the restart should not be less than this time, and fuel cell minimum on time to avoid frequent on/off cycles. The charge sustenance of the battery is also sought through adjusting the fuel cell current based on battery SOC.

$$I_{fc} = \begin{cases} I_{min} & \mathrm{I}_{ch} + I_d < I_{min} \\ I_{ch}(ba_{SOC}) + I_d & I_{min} \leq I_{ch} + I_d \leq I_{max} \\ I_{max} & \mathrm{I}_{ch} + I_d > I_{max} \end{cases} \tag{62}$$

when fuel cell current is decided by the LFCS, the supercapacitor current

is decided by supercapacitor SOC and the difference between fuel cell reference current and power demand of drive cycle. The flow chart of OMCS to determine supercapacitor current is shown as figure 15. When fuel cell current and battery current are decided, battery current is passively decided by the difference between current demand, fuel cell current and supercapacitor current on DC bus.

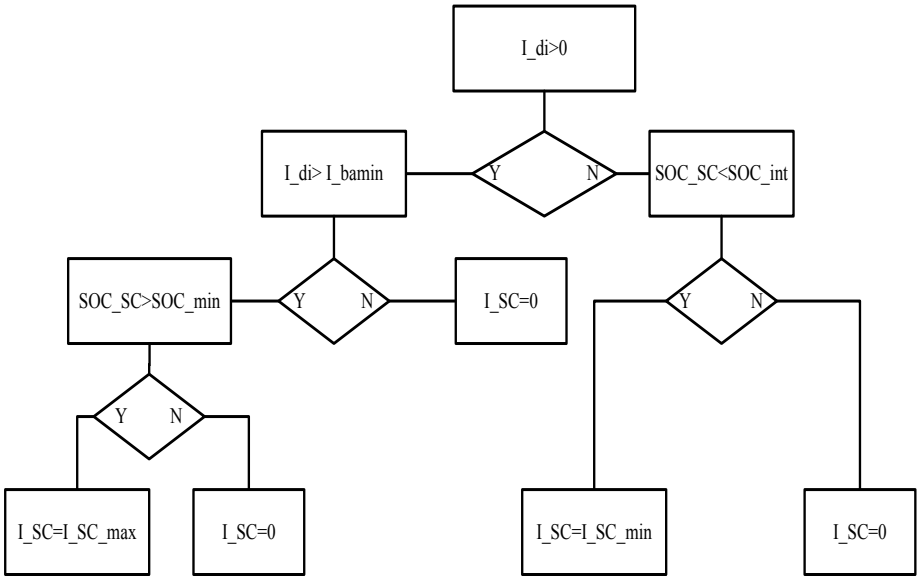


Figure 15: Flowchart of OMCS

Due to low energy density and the role of supercapacitor as peak power supplier, many research on ECMS simplifies the equivalent hydrogen consumption of supercapacitor into null. To prove that the simplification of ECMS cannot reach the optimal resolution, an HEOS is designed. The first part of HEOS is simplified ECMS to calculate fuel cell current and the second part is OMCS to calculate supercapacitor current. Three control strategies are tested using the described test bench and experiment results are shown as Table 3.

According to Table 3, final battery SOCs of all three strategies are above the 0.79, which is defined as the criteria value that whether the battery satisfies charge-sustenance requirement. Hydrogen consumption by fuel cell at the end

Table 3: Experiment results

| EMSs | ECMS | RBCS | HEOS |
|---|---|---|---|
| Initial supercapacitor and battery SOC | 0.8 | 0.8 | 0.8 |
| Final supercapacitor SOC | 0.5865 | 0.8304 | 0.8199 |
| Final battery SOC | 0.7915 | 0.7946 | 0.7906 |
| First hydrogen consumption (L) | 194.07 | 210.35 | 194.77 |
| Final hydrogen consumption (L) | 225.06 | 230.02 | 228.42 |

of drive cycle is defined as the first hydrogen consumption. Regarding different battery final SOC values at the end of the drive cycle, fuel cell is continued to operate at maximum efficiency point to charge the battery until its final SOC reaches to 0.8. Meanwhile, the supercapacitor is charged or discharged to let its final SOC be equal to 0.8. When all SOCs of energy storage sources are 0.8, the fuel cell stops working, the hydrogen consumption is defined as the final hydrogen consumption. It can be observed that the ECMS has least final hydrogen consumption, which proves its superiority.

## 5. Power sources degradation and AECMS

### *5.1. The effect of power sources degradation on ECMS*

Along with fuel cell degradation, the fuel cell output voltage decreases, but auxiliary power doesn't change, so efficiency decreases. When fuel cell is fully degraded, that its SOH is equal to 1, the efficiency changes as Figure 16.

It can be observed that the efficiency of the aged fuel cell is all less than the new one. The maximum efficiency decreases from 42.83% to 41.37%, but the maximum efficiency point occurs at the same current point 9.5A. So, the parameter $\eta_{opt}$ and $\eta_{max}$ of $K_{FC}$ should tune with fuel cell degradation degree.

In order to analyze the effects of power sources degradation on the designed ECMS, four degradation conditions of fuel cell and battery are considered as Table 4. The simulation results for four conditions are shown as Figure 17, in order to be convenient to describe different conditions, they are defined as FHBH,

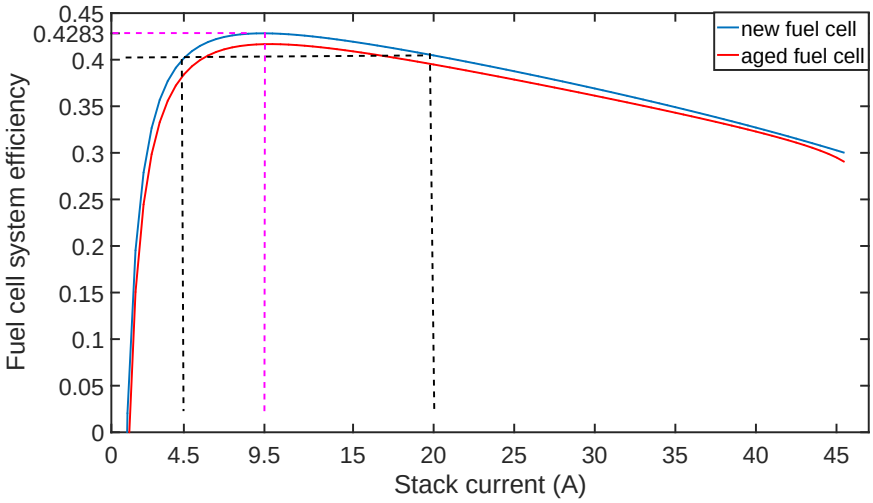


Figure 16: Comparative results of fuel cell system efficiency between the new fuel cell and aged one

FDBH, FHBD and FDBD respectively. The simulation results are shown as Table 5. Every condition is analyzed respectively in detail.

Table 4: Four degradation conditions of power sources

| Condition | $SOH_{FC}$ | $SOH_{BA}$ |
|---|---|---|
| FHBH | 0 | 0 |
| FHBD | 0 | 1 |
| FDBH | 1 | 0 |
| FDBD | 1 | 1 |

From Figure 17 and Table 5, it can be observed that the fuel cell of FHBH starts at 443s and it fluctuates around the maximum efficiency point due to battery and supercapacitor SOC variations. The battery final SOC is almost equal to its initial value. FHBH has the least maximum battery SOC variation which is defined as the difference between maximum battery SOC and minimum battery SOC during the whole drive cycle period.

Compared to FHBH, the fuel cell of FHBD starts earlier, the battery final

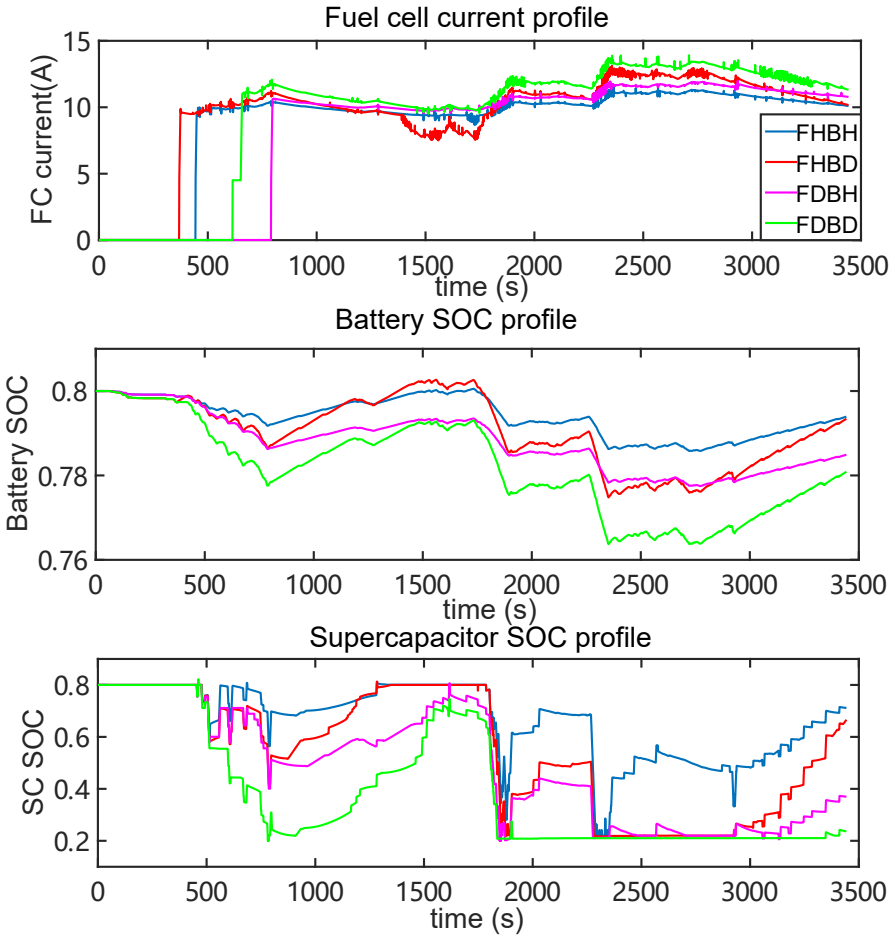


Figure 17: Comparative results of ECMS under four power sources degradation conditions

Table 5: Simulation results of ECMS for four conditions

| | FHBH | FDBH | FHBD | FDBD |
|---|---|---|---|---|
| hydrogen consumption (g) | 15.1 | 14.0 | 16.0 | 16.1 |
| battery initial SOC | 0.8 | 0.8 | 0.8 | 0.8 |
| battery final SOC | 0.7939 | 0.7849 | 0.7934 | 0.7809 |
| battery SOC variation | 0.0147 | 0.0225 | 0.0279 | 0.363 |
| supercapacitor initial SOC | 0.8 | 0.8 | 0.8 | 0.8 |
| supercapacitor final SOC | 0.7115 | 0.3699 | 0.6661 | 0.2363 |
| supercapacitor SOC variation | 0.5884 | 0.6072 | 0.5969 | 0.6223 |

SOC is almost equal to FHBH. But due to the decrease of battery capacity and the increase of battery resistance along with its degradation, the battery SOC variation for the whole drive cycle is larger than FHBH, meanwhile, this also leads to larger fluctuation amplitude of fuel cell current. Final hydrogen consumption of FHBD is 16g increasing 5.625% than FHBH.

Compared to the other three conditions, the fuel cell of FDBH starts at the latest, which is due to the decrease of fuel cell efficiency and the increase of EF. The lower battery SOC is needed to trigger the operation of fuel cell. The fuel cell current of FDBH is larger than FHBH on the whole due to low battery SOC. Final battery SOC FDBH is 0.7849 and the difference between the initial and final value increases by 59.6% than FHBH, which cannot meet the battery charge sustenance requirement.

FDBD has the largest battery and supercapacitor SOC variations and the final SOCs are the least. FDBD also has the most hydrogen consumption and fuel cell current is larger than the other three conditions when fuel cell is started.

Through the analysis of four degradation conditions, it can be concluded that compared to the health state, the battery degradation leads to more variable battery SOC, more fluctuation of fuel cell current around maximum efficiency point, more hydrogen consumption and earlier fuel cell start-up, but final battery SOC is not affected. Fuel cell degradation makes its maximum efficiency

value decrease but corresponding fuel cell current doesn't change. The trigger time of fuel cell start-up is delayed and battery final SOC changes much to the initial SOC, which cannot be allowed for the charge sustenance of FCHEV. At the real situation, fuel cell and battery degrade together and the operation results of the vehicle are worse than single power source degradation.

### *5.2. Adaptive equivalent consumption minimization strategy*

EF is an important parameter for ECMS. For an assigned known driving mission, a constant equivalent factor is enough to reach an optimal solution. But when fuel cell and battery degrade, the former constant equivalent factor cannot guarantee the charge sustenance of ESSs and optimal fuel consumption. In order to solve this problem, AECMS is proposed by adjusting EF according to SOHs of power sources [61]. The variation of equivalent factors is defined as equation (63)(64).

$$\lambda_{BA} = \lambda_{BA0}\left(1 + 0.193SOH_{FC}\right)\left(1 + 0.193SOH_{BA}\right) \tag{63}$$

$$\lambda_{SC} = \lambda_{SC0}\left(1 + 0.193SOH_{FC}\right)\left(1 + 0.193SOH_{BA}\right) \tag{64}$$

where $\lambda_{BA0}$ and $\lambda_{SC0}$ are initial battery and supercapacitor EFs.

The degradation of battery leads to the increase of fuel cell current variation in the whole drive cycle, which means the increase of fuel cell degradation rate. In order to increase fuel cell lifetime, the limitation on its dynamic change rate in equation (55) is adjusted according to battery SOH as equation (65).

$$dI = dI_0 * \left(1 - 0.5 * SOH_{BA}\right) \tag{65}$$

The architecture of the AECMS control system for FCHEV is shown in Figure 18. Based on the built degradation model of power sources and UKF, their SOHs are estimated. The equivalent factor and dynamic change rate of fuel cell are changed according to their SOHs to make sure the normal operation of the vehicle, increase the durability of power sources, and keep the stability of control system.

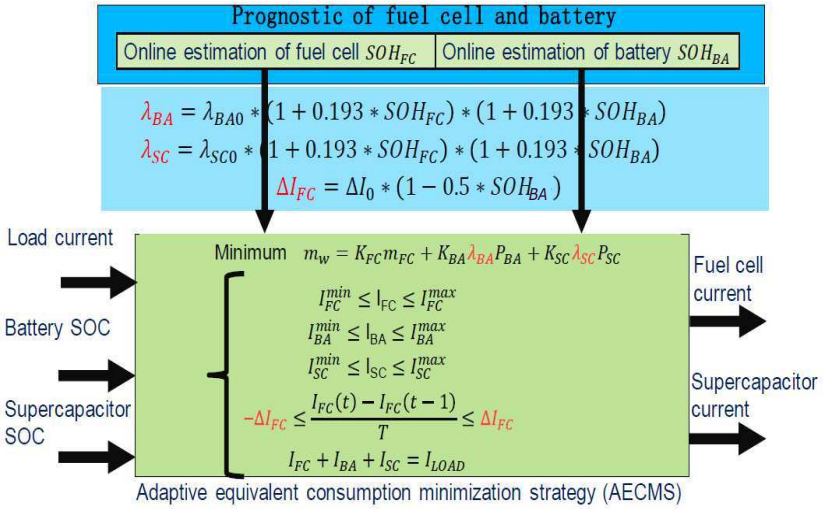


Figure 18: Control system of AECMS for FCHEV

601 The simulation results of AECMS are shown in Figure 19 and Table 6.

Table 6: Simulation results of AECMS for four conditions

| | FHBH | FDBH | FHBD | FDBD |
|---|---|---|---|---|
| hydrogen consumption (g) | 15.1 | 17.7 | 17.4 | 19.8 |
| battery initial SOC | 0.8 | 0.8 | 0.8 | 0.8 |
| battery final SOC | 0.7939 | 0.7953 | 0.8 | 0.8 |
| battery SOC variation | 0.0147 | 0.0157 | 0.0245 | 0.0258 |
| supercapacitor initial SOC | 0.8 | 0.8 | 0.8 | 0.8 |
| supercapacitor final SOC | 0.7113 | 0.7620 | 0.8 | 0.8 |
| supercapacitor SOC variation | 0.5884 | 0.5967 | 0.6183 | 0.6032 |

602 From Figure 19, it can be observed that the simulation results of the con-
603 dition FHBH are same for ECMS and AECMS. For condition FDBH, the start
604 time of fuel cell changes from the latest for ECMS to the earliest for AECMS and
605 the fuel cell current is around maximum efficiency point. Regarding FHBD and
606 FDBD, the start time is put off and fuel cell current gets larger. The increase of

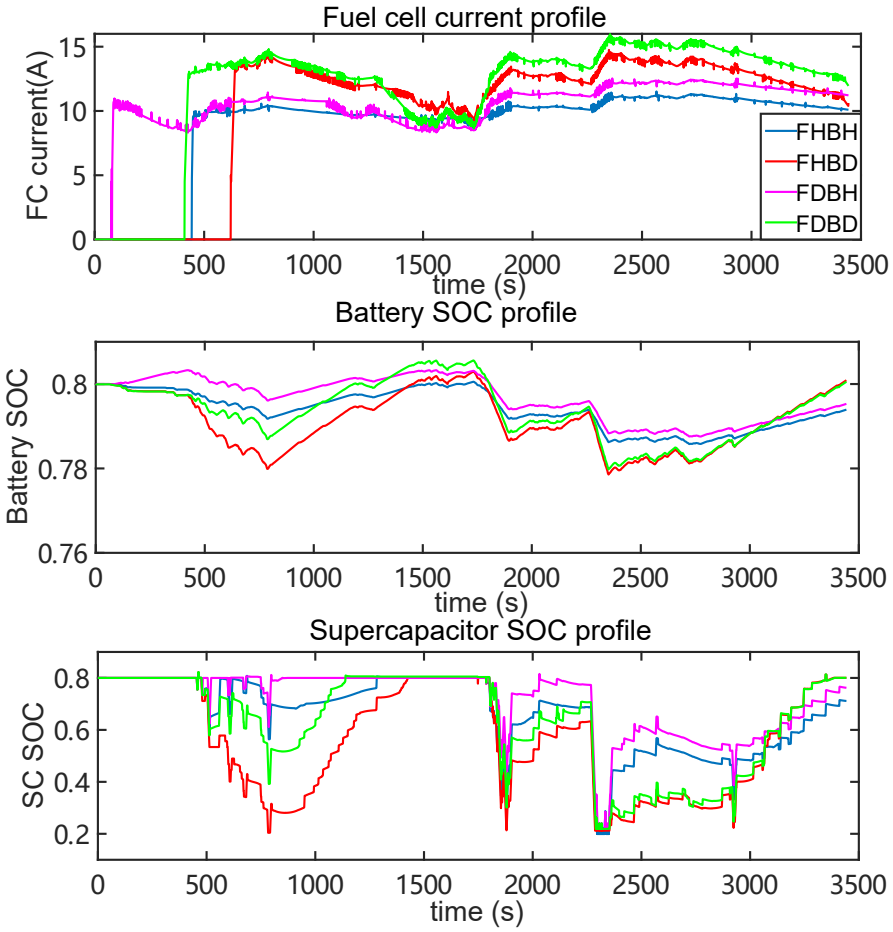


Figure 19: Comparative results of AECMS under four degradation conditions of power sources

adaptive equivalent factor along with power sources degradation advances the start of fuel cell. The decrease of dynamic change rate along with battery SOH delays the start of fuel cell and makes the increase of fuel cell current. Table 6 shows that all battery final SOCs for four degradation conditions are above 0.79 meaning that the charge sustaining requirement of energy storage sources is met.

Same to ECMS, AECMS has play the full potential of fuel cell, battery and supercapacitor: fuel cell supplies steady energy and seeks for the maximum efficiency in the high efficiency zone, battery is operated as the main energy buffer and its charge sustenance is kept at the end of drive cycle and supercapacitor supplies peak power. The designed AECMS can make sure the normal operation of a vehicle even though power sources have degraded seriously. It should be mentioned that when fuel cell and battery SOHs reach 1, it doesn't mean the fuel cell and battery cannot work anymore and it just shows that the probability of the failure of power sources is very high. In case of bringing serious damage to the vehicle, power sources should be replaced in advance.

## 6. Conclusion

In this paper, an ECMS strategy is designed for the FCHEV. Under the guidance of ECMS, three power sources full play their potential: Fuel cell as the main power source is operated to seek for the maximum efficiency point in the defined high efficiency zone, while the battery is taken as the main energy storage source to buffer energy demand by vehicle and the supercapacitor is dedicated to providing the peak power. Considering low energy density of supercapacitor, its equivalent hydrogen consumption is neglected by many ECMSs which leading to more hydrogen consumption and complex of the control system. This paper takes all three power sources into the objective function.

In order to prove the validity of the ECMS, an experimental test bench is built and two comparative control strategies: RBCS and HEOS are designed. The WVUCITY, New York Bus and LA92 drive cycles have been emulated on an

experimental test bench with the three above control strategies. The experiment results show that the proposed ECMS has the least hydrogen consumption and it offers the longest durability of fuel cell. Along with vehicle operation, fuel cell and battery degrade, which brings the crisis of optimization and reliability to the EMS. For the ECMS, the maximum efficiency point, and optimal EF value are changed. The aging models of the fuel cell and the battery are built, and the on-line prognostic approach is designed. According to the real-time SOH value of fuel cell and battery, the designed novel AECMS adjust the EFs and fuel cell dynamic current rate to make sure the normal operation of the vehicle. In the future, the optimal coefficients of the equivalent factor and dynamic change rate of fuel cell current will be studied.

## References


[1] N. Sulaiman, M. A. Hannan, A. Mohamed, E. H. Majlan, W. R. Wan Daud, A review on energy management system for fuel cell hybrid electric vehicle: Issues and challenges, Renewable and Sustainable Energy Reviews 52 (2015) 802–814.

[2] H. S. Das, C. W. Tan, A. H. M. Yatim, Fuel cell hybrid electric vehicles: A review on power conditioning units and topologies, Renewable and Sustainable Energy Reviews 76 (2017) 268–291.

[3] C. Manzie, O. Grondin, A. Sciarretta, G. Zito, Ecms controller robustness in flex-fuel hybrid vehicles, Journal of Dynamic Systems, Measurement, and Control 136 (6) (2014) 064504.

[4] H. Wang, Y. Huang, H. He, C. Lv, W. Liu, A. Khajepour, Energy Management of Hybrid Electric Vehicles, 2018, pp. 159–206.

[5] Z. Hong, Q. Li, Y. Han, W. Shang, Y. Zhu, W. Chen, An energy management strategy based on dynamic power factor for fuel cell/battery hybrid locomotive, International Journal of Hydrogen Energy 43 (6) (2018) 3261–3272.

[6] N. Jalil, N. A. Kheir, M. Salman, A rule-based energy management strategy for a series hybrid vehicle, in: Proceedings of the 1997 American Control Conference (Cat. No.97CH36041), Vol. 1, pp. 689–693 vol.1. doi:10.1109/ACC.1997.611889.

[7] S. Ahmadi, S. M. T. Bathaee, Multi-objective genetic optimization of the fuel cell hybrid vehicle supervisory system: Fuzzy logic and operating mode control strategies, International Journal of Hydrogen Energy 40 (36) (2015) 12512–12521.

[8] A. Fadel, B. Zhou, An experimental and analytical comparison study of power management methodologies of fuel cell–battery hybrid vehicles, Journal of Power Sources 196 (6) (2011) 3271–3279.

[9] I. Lachhab, L. Krichen, An improved energy management strategy for fc/uc hybrid electric vehicles propelled by motor-wheels, International Journal of Hydrogen Energy 39 (1) (2014) 571–581. doi:10.1016/j.ijhydene.2013.10.064.

[10] H. Aouzellag, K. Ghedamsi, D. Aouzellag, Energy management and fault tolerant control strategies for fuel cell/ultra-capacitor hybrid electric vehicles to enhance autonomy, efficiency and life time of the fuel cell system, International Journal of Hydrogen Energy 40 (22) (2015) 7204–7213. doi:http://dx.doi.org/10.1016/j.ijhydene.2015.03.132.

[11] H. Yun, S. Liu, Y. Zhao, J. Xie, C. Liu, Z. Hou, K. Wang, Energy management for fuel cell hybrid vehicles based on a stiffness coefficient model, International Journal of Hydrogen Energy 40 (1) (2015) 633–641.

[12] Q. Li, H. Yang, Y. Han, M. Li, W. Chen, A state machine strategy based on droop control for an energy management system of pemfc-battery-supercapacitor hybrid tramway, International Journal of Hydrogen Energy 41 (36) (2016) 16148–16159.

[13] J.-J. Hwang, J.-S. Hu, C.-H. Lin, Design of a range extension strategy for power decentralized fuel cell/battery electric vehicles, International Journal of Hydrogen Energy 40 (35) (2015) 11704–11712.

[14] Q. Li, W. Chen, Y. Li, S. Liu, J. Huang, Energy management strategy for fuel cell/battery/ultracapacitor hybrid vehicle based on fuzzy logic, International Journal of Electrical Power & Energy Systems 43 (1) (2012) 514–525.

[15] H. Li, A. Ravey, A. N. Diaye, A. Djerdir, A review of energy management strategy for fuel cell hybrid electric vehicle, in: 2017 IEEE Vehicle Power and Propulsion Conference (VPPC), pp. 1–6. doi:10.1109/VPPC.2017.8330970.

[16] S. F. Tie, C. W. Tan, A review of energy sources and energy management system in electric vehicles, Renewable and Sustainable Energy Reviews 20 (2013) 82–102.

[17] N. Sulaiman, M. A. Hannan, A. Mohamed, P. J. Ker, E. H. Majlan, W. R. Wan Daud, Optimization of energy management system for fuel-cell hybrid electric vehicles: Issues and recommendations, Applied Energy 228 (2018) 2061–2079.

[18] S. Zhang, R. Xiong, Adaptive energy management of a plug-in hybrid electric vehicle based on driving pattern recognition and dynamic programming, Applied Energy 155 (2015) 68–78.

[19] C. Wilke, A. Bensmann, S. Martin, A. Utz, R. Hanke-Rauschenbach, Optimal design of a district energy system including supply for fuel cell electric vehicles, Applied Energy 226 (2018) 129–144.

[20] P. Zhang, F. Yan, C. Du, A comprehensive analysis of energy management strategies for hybrid electric vehicles based on bibliometrics, Renewable and Sustainable Energy Reviews 48 (2015) 88–104.

[21] S.-Y. Chen, Y.-H. Hung, C.-H. Wu, S.-T. Huang, Optimal energy management of a hybrid electric powertrain system using improved particle swarm optimization, Applied Energy 160 (2015) 132–145.

[22] P. García, J. P. Torreglosa, L. M. Fernández, F. Jurado, Viability study of a fc-battery-sc tramway controlled by equivalent consumption minimization strategy, International Journal of Hydrogen Energy 37 (11) (2012) 9368–9382.

[23] W. Zhang, J. Li, L. Xu, M. Ouyang, Optimization for a fuel cell/battery/capacity tram with equivalent consumption minimization strategy, Energy Conversion and Management 134 (Supplement C) (2017) 59 – 69.

[24] P. García, J. P. Torreglosa, L. M. Fernández, F. Jurado, Control strategies for high-power electric vehicles powered by hydrogen fuel cell, battery and supercapacitor, Expert Systems with Applications 40 (12) (2013) 4791–4804.

[25] H. Li, A. Ravey, A. N'Diaye, A. Djerdir, A novel equivalent consumption minimization strategy for hybrid electric vehicle powered by fuel cell, battery and supercapacitor, Journal of Power Sources 395 (2018) 262–270. doi:10.1016/j.jpowsour.2018.05.078.

[26] S. Pelletier, O. Jabali, G. Laporte, M. Veneroni, Battery degradation and behaviour for electric vehicles: Review and numerical analyses of several models, Transportation Research Part B-Methodological 103 (2017) 158–187.

[27] T. Sutharssan, D. Montalvao, Y. K. Chen, W. C. Wang, C. Pisac, H. Elemara, A review on prognostics and health monitoring of proton exchange membrane fuel cell, Renewable and Sustainable Energy Reviews 75 (2017) 440–450.

[28] L. Zhang, X. Hu, Z. Wang, F. Sun, D. G. Dorrell, A review of supercapacitor modeling, estimation, and applications: A control/management perspective, Renewable and Sustainable Energy Reviews 81 (Part 2) (2018) 1868–1878.

[29] J. Solano, D. Hissel, M. Pera, Fail-safe power for hybrid electric vehicles: Implementing a self-sustained global energy management system, IEEE Vehicular Technology Magazine 13 (2) (2018) 34–39. doi:10.1109/MVT.2017.2776670.

[30] C. Yang, S. Du, L. Li, S. You, Y. Yang, Y. Zhao, Adaptive real-time optimal energy management strategy based on equivalent factors optimization for plug-in hybrid electric vehicle, Applied Energy 203 (2017) 883–896. doi:https://doi.org/10.1016/j.apenergy.2017.06.106.

[31] C. Sun, F. Sun, H. He, Investigating adaptive-ecms with velocity forecast ability for hybrid electric vehicles, Applied Energy 185 (2017) 1644–1653. doi:https://doi.org/10.1016/j.apenergy.2016.02.026.

[32] L. Guzzella, A. Sciarretta, Vehicle Propulsion Systems, Introdution to modeling and optimization, 1st Edition, Springer, 2005.

[33] J. Kim, M. Kim, T. Kang, Y.-J. Sohn, T. Song, K. H. Choi, Degradation modeling and operational optimization for improving the lifetime of high-temperature pem (proton exchange membrane) fuel cells, Energy 66 (2014) 41–49.

[34] G. Fei, B. Blunier, A. Miraoui, Pem fuel cell stack modeling for real-time emulation in hardware-in-the-loop applications, IEEE Transactions on Energy Conversion 26 (1) (2011) 184–194.

[35] H. Li, A. Ravey, A. N'Diaye, A. Djerdir, Equivalent consumption minimization strategy for hybrid electric vehicle powered by fuel cell, battery and supercapacitor, in: IECON 2016 - 42nd Annual Conference of the IEEE Industrial Electronics Society, 2016, pp. 4401–4406.

[36] M. Basualdo, D. Feroldi, R. Outbib, Pem fuel cells with bio-ethanol processor systems, Springer 10 (2012) 978–1.

[37] C. H. Zheng, C. E. Oh, Y. I. Park, S. W. Cha, Fuel economy evaluation of fuel cell hybrid vehicles based on equivalent fuel consumption, International Journal of Hydrogen Energy 37 (2) (2012) 1790–1796.

[38] D. Zhao, F. Gao, P. Massonnat, M. Dou, A. Miraoui, Parameter sensitivity analysis and local temperature distribution effect for a pemfc system, IEEE Transactions on Energy Conversion 30 (3) (2015) 1008–1018. doi:10.1109/tec.2015.2404793.

[39] C. Zheng, C. Oh, Y. Park, S. Cha, Fuel economy evaluation of fuel cell hybrid vehicles based on equivalent fuel consumption, International Journal of Hydrogen Energy 37 (2) (2012) 1790 – 1796, 10th International Conference on Clean Energy 2010.

[40] M. J. Daigle, C. S. Kulkarni, Electrochemistry-based battery modeling for prognostics.

[41] R. R. Richardson, M. A. Osborne, D. A. Howey, Gaussian process regression for forecasting battery state of health, Journal of Power Sources 357 (2017) 209–219.

[42] B. Bole, C. S. Kulkarni, M. Daigle, Adaptation of an electrochemistry-based li-ion battery model to account for deterioration observed under randomized use, Tech. rep., SGT, Inc. Moffett Field United States (2014).

[43] D. K. Karthikeyan, G. Sikha, R. E. White, Thermodynamic model development for lithium intercalation electrodes, Journal of Power Sources 185 (2) (2008) 1398–1407. doi:10.1016/j.jpowsour.2008.07.077.

[44] K. Sang-Hyun, C. Woojin, L. Kyo-Bum, C. Sewan, Advanced dynamic simulation of supercapacitors considering parameter variation and self-discharge, IEEE Transactions on Power Electronics 26 (11) (2011) 3377–3385.

[45] R. L. Spyker, R. M. Nelms, Classical equivalent circuit parameters for a double-layer capacitor, IEEE Transactions on Aerospace and Electronic Systems 36 (3) (2000) 829–836.

[46] S. Sankararaman, M. J. Daigle, K. Goebel, Uncertainty quantification in remaining useful life prediction using first-order reliability methods, IEEE Transactions on Reliability 63 (2) (2014) 603–619.

[47] M. Daigle, B. Saha, K. Goebel, A comparison of filter-based approaches for model-based prognostics, in: 2012 IEEE Aerospace Conference, 2012, pp. 1–10.

[48] E. A. Wan, R. V. D. Merwe, The unscented kalman filter for nonlinear estimation, in: Proceedings of the IEEE 2000 Adaptive Systems for Signal Processing, Communications, and Control Symposium (Cat. No.00EX373), 2000, pp. 153–158.

[49] G. Sierra, M. Orchard, K. Goebel, C. Kulkarni, Battery health management for small-size rotary-wing electric unmanned aerial vehicles: An efficient approach for constrained computing platforms, Reliability Engineering & System Safety 182 (2019) 166–178.

[50] H. Li, A. Ravey, A. N'Diaye, A. Djerdir, State of health estimation of lithium-ion batteries under variable load profile, in: IECON 2017 - 43rd Annual Conference of the IEEE Industrial Electronics Society, 2017, pp. 5287–5291.

[51] R. Yang, R. Xiong, H. He, H. Mu, C. Wang, A novel method on estimating the degradation and state of charge of lithium-ion batteries used for electrical vehicles, Applied Energy 207 (2017) 336–345. doi:10.1016/j.apenergy.2017.05.183.

[52] P. Gazdzick, J. Mitzel, D. Garcia Sanchez, M. Schulze, K. A. Friedrich, Evaluation of reversible and irreversible degradation rates of polymer elec-

trolyte membrane fuel cells tested in automotive conditions, Journal of Power Sources 327 (2016) 86–95.

[53] J. Larminie, A. Dicks, Fuel Cell Systems Explained, J. Wiley, 2003.

[54] M. Jouin, R. Gouriveau, D. Hissel, M.-C. Péra, N. Zerhouni, Degradations analysis and aging modeling for health assessment and prognostics of pemfc, Reliability Engineering & System Safety 148 (2016) 78–95.

[55] M. Bressel, M. Hilairet, D. Hissel, B. O. Bouamama, Remaining useful life prediction and uncertainty quantification of proton exchange membrane fuel cell under variable load, IEEE Transactions on Industrial Electronics 63 (4) (2016) 2569–2577.

[56] M. Bressel, M. Hilairet, D. Hissel, B. Ould Bouamama, Extended kalman filter for prognostic of proton exchange membrane fuel cell, Applied Energy 164 (2016) 220–227.

[57] R. Ma, T. Yang, E. Breaz, Z. Li, P. Briois, F. Gao, Data-driven proton exchange membrane fuel cell degradation predication through deep learning method, Applied Energy 231 (2018) 102–115.

[58] Y. Xie, A. Savvaris, A. Tsourdos, Fuzzy logic based equivalent consumption optimization of a hybrid electric propulsion system for unmanned aerial vehicles, Aerospace Science and Technology 85 (2019) 13–23.

[59] R. Fletcher, The Sequential Quadratic Programming Method, Springer Berlin Heidelberg, Berlin, Heidelberg, 2010, pp. 165–214.

[60] K. Ettihir, M. Higuita Cano, L. Boulon, K. Agbossou, Design of an adaptive ems for fuel cell vehicles, International Journal of Hydrogen Energydoi:10.1016/j.ijhydene.2016.07.211.

[61] J. Han, Y. Park, D. Kum, Optimal adaptation of equivalent factor of equivalent consumption minimization strategy for fuel cell hybrid electric vehicles under active state inequality constraints, Journal of Power Sources 267 (2014) 491–502.

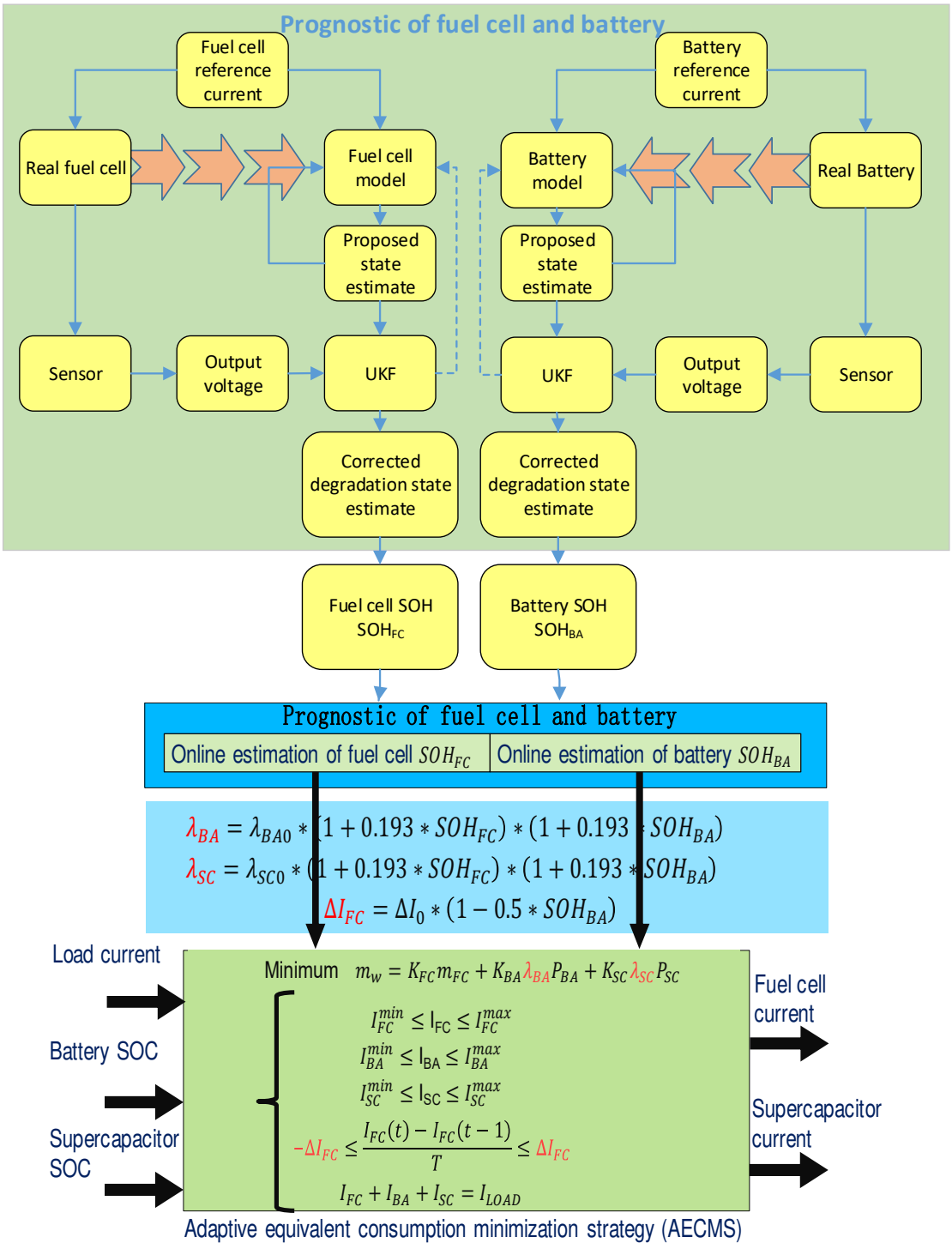
Prognostic of fuel cell and battery
Fuel cell reference current
Battery reference current
Real fuel cell
Fuel cell model
Battery model
Real Battery
Proposed state estimate
Proposed state estimate
Sensor
Output voltage
UKF
UKF
Output voltage
Sensor
Corrected degradation state estimate
Corrected degradation state estimate
Fuel cell SOH $SOH_{FC}$
Battery SOH $SOH_{BA}$
Prognostic of fuel cell and battery
Online estimation of fuel cell $SOH_{FC}$
Online estimation of battery $SOH_{BA}$
$\lambda_{BA} = \lambda_{BA0} * (1 + 0.193 * SOH_{FC}) * (1 + 0.193 * SOH_{BA})$
$\lambda_{SC} = \lambda_{SC0} * (1 + 0.193 * SOH_{FC}) * (1 + 0.193 * SOH_{BA})$
$\Delta I_{FC} = \Delta I_0 * (1 - 0.5 * SOH_{BA})$
Load current
Battery SOC
Supercapacitor SOC
Minimum $m_w = K_{FC} m_{FC} + K_{BA} \lambda_{BA} P_{BA} + K_{SC} \lambda_{SC} P_{SC}$
$I_{FC}^{min} \le I_{FC} \le I_{FC}^{max}$
$I_{BA}^{min} \le I_{BA} \le I_{BA}^{max}$
$I_{SC}^{min} \le I_{SC} \le I_{SC}^{max}$
$-\Delta I_{FC} \le \frac{I_{FC}(t) - I_{FC}(t-1)}{T} \le \Delta I_{FC}$
$I_{FC} + I_{BA} + I_{SC} = I_{LOAD}$
Fuel cell current
Supercapacitor current
Adaptive equivalent consumption minimization strategy (AECMS)